Multi-Body Vehicle Dynamics Modeling for Drift Analysis

by

Francis Loh

A thesis
presented to the University of Waterloo
in fulfillment of the
thesis requirement for the degree of
Master of Applied Science
in
Systems Design Engineering

Waterloo, Ontario, Canada, 2013

I hereby declare that I am the sole author of this thesis. This is a true copy of the thesis, including any required final revisions, as accepted by my examiners.

I understand that my thesis may be made electronically available to the public.

Abstract

One area of vehicle handling performance that has been the focus of an OEM's (Original Equipment Manufacturer) engineering effort is within the realm of vehicle straight-line performance. As the name implies, straight-line performance is determinant on the vehicle's tendency to resist vehicle lateral drift when being driven straight. Vehicle lateral drift is a condition where the driver must apply a constant correctional torque to the steering wheel in order to maintain a straight line course.

A full vehicle model was developed to simulate the influences of suspension parameters on vehicle drift. Adams 2010 was chosen as the multi-body dynamics (MBD) software for this research for its ability to develop a full vehicle high fidelity model without the need for physical test data. The model was created from standard Adams/Car suspension templates modified to accommodate the subject vehicle. The front suspension sub-assembly model was built upon the front MacPherson strut suspension template. Likewise, the rear suspension sub-assembly model was created from the rear multi-link suspension template.

The tire model used in the full vehicle model was based on the Pacejka 2002 formulation. A model of a similar tire was generated using a custom spreadsheet based on the PAC2002, a slightly modified version of the Pacejka 2002 formulation found within Adams/Car. A virtual tire test rig and a 6/7-DoF model were created to understand and verify the behaviour of the generated tire models. The virtual tire test rig was used to compare the outputs of the PAC2002 tire model to the calculated values from a custom tire property spreadsheet. The 6/7-DoF model was used to test and verify the effect of the tires residual lateral forces.

The full-vehicle model was verified using the parallel wheel travel and opposite wheel travel suspension analyses. The parallel wheel travel analysis was used to tease out binding

issues within the designed travel of the suspension. The opposite wheel travel analysis was used similarly for anti-roll bar systems.

Simulations based on the industry standard vehicle drift tests were run to understand the effect of certain vehicle suspension geometry on vehicle drift, namely the vehicles front and rear camber and toe angles. The full-vehicle model was also subjected to straight-line performance simulations with various road bank or crown angles. The results were compared with industry-standard vehicle drift test data gathered by the OEM on their own test track. The results indicate that the direction of vehicle pull matches with the OEM test data, but the magnitudes differ in both the positively and negatively banked road simulation results. It is likely that the difference in vehicle drift is due to the lack of steering data obtained for the full-vehicle model.

Acknowledgements

I would like to express my sincere appreciation and gratitude to my thesis supervisors, Professor John McPhee and Dr. Chad Schmitke in the Department of Systems Design Engineering, for their continued support and guidance towards the completion of my Masters degree. They have been the backbone of my work presented in this thesis paper, and their knowledge and understanding of vehicle dynamics has never failed to impress me.

In addition, I am grateful to my thesis readers, Professor Steve Lambert in the Department of Mechanical Engineering and Professor Nasser Lashgarian Azad in the Department of Systems Design Engineering for their rigorous review of my work. Without their helpful constructive criticism, I would not have been able to produce this work.

This research has been supported financially by an automotive orignal equiment manufacturer (OEM), of which the name is left anonymous for confidentiality. I would like to mention that Ryan Kim and Koichi Sugiyama from the OEM have contributed greatly to my research by providing valuable documentation and specifications.

Finally, I would like to thank my family for their unconditional support throughout this arduous journey.

Table of Contents

List of Tables

List of Figures

Chapter 1

Introduction

1.1 Background

The consumer market has become more accustomed to having their expectations met, whether it is for services rendered or product performance. Consumer expectations have not only driven demand for resources significantly higher, but they have also forced product manufacturers to innovate their art of engineering. One area of innovation that has received an increasing amount of attention in modern day engineering is modeling and simulation.

With the advent of powerful computational devices, modern engineering processes have been relying increasingly on simulations. Design and manufacturing changes can be evaluated at correlated levels of confidence without incurring the high costs associated with physical testing. Also, the time required to obtain similar results are significantly reduced, allowing engineers to directly implement changes during the design process or on the manufacturing floor.

The engineering simulation process mainly consists of designing an idealized model

of the system, generating results from the model, validating the results and generating "what if" simulations. The process begins with the design of an idealized model of the system. In this crucial step, the important characteristics and parameters are identified and designed into the model as elements, such as physical representations, forces and torques, interactions etc. The ability to reduce the number of such elements at this stage to generate the required outputs will decrease the complexity and computing time in subsequent steps. Also within this step, elements are formed as equations to develop the idealized system. Similarly, efficient packaging of the system of equations will yield a decrease in complexity and computing time. The second step requires solving the system of equations to generate the necessary outputs as defined in the first step. It is important to select a solver that will yield the values within an expected tolerance for a reasonable amount of computational time. In the final step, the idealized model will be validated by correlating the generated results to physical testing. This iterative process will ultimately tune the parameters of the idealized model to allow it to predict characteristics with untested inputs, but within the range of tested values.

The presented upsides of engineering simulations may have created the pretense of a perfect solution fallacy. However, it is important to understand that the accuracy and relevance of the simulation results from a validated model rests mainly on quality of the input data. It is not unusual for modern engineers to accept the output values without analyzing the input data, which can be clouded with external factors that were not included in the validated model.

The application of modeling and simulations in the automotive industry has been increasingly widespread. Automotive engineers are utilizing sophisticated software packages to predict mechanical failures, fluid flow characteristics, thermal dynamics, and multibody dynamics and kinematics. In the realm of vehicle dynamics, a subset of multibody

dynamics and kinematics, engineers have access to a variety of software tools to design and test vehicle suspension concepts. These tools include mathematical and geometrical models, on-board data acquisition systems, full vehicle test rigs, and component test machines [31]. Vehicle models are based on mathematical and geometrical equations and can be created using multibody dynamics software such as MSC.Adams and MapleSim, or using automotive industry specific software such as CarSim. To provide the models with input parameters, full vehicle test rigs and vehicle component test machines are utilized to obtain relevant data. Also, on-board data acquisition systems can gather data to tune and validate the vehicle model.

In modern day vehicle engineering, vehicle dynamics software packages have been playing a more significant role throughout the design process. Larger available computing power has allowed automotive manufacturers to design, test and optimize a vehicle prior to assembly. However, a full vehicle model can also be useful within the manufacturing process. Manufacturing engineers will be able to model the effect of manufacturing tolerances on vehicle handling performance, or be able to diagnose related customer complaints.

One area of vehicle handling performance that has been the focus of an OEM's (Original Equipment Manufacturer) engineering effort is within the realm of vehicle straight-line performance. As the name implies, straight-line performance is determinant on the vehicle's tendency to resist vehicle lateral drift when being driven straight. Vehicle lateral drift is a condition where the driver must apply a constant correctional torque to the steering wheel in order to maintain a straight line course [4]. The OEM identified this as an area for improvement and outlined a plan to include a partnership between the University of Waterloo to collaborate and develop a full vehicle model of one of their sport utility vehicles (SUV). For the purpose of confidentiality, the OEM's identity and the vehicle model are kept anonymous within this thesis.

1.2 Problem Statement

The ability for a vehicle to travel along a straight line with no external driver input is important for safe and comfortable driving. If the vehicle were to stray from this line, this measured deviation is known as vehicle drift. With vehicle drift, the predictability of the vehicle's heading is negatively decreased, and as such, the driver has to apply corrective steering to maintain a straight-line path. For longer drives, this can be tiresome and dangerous.

In 2009, the management team of the OEM decided to focus their efforts on improving the SUV's straight-line performance. This will be achieved by understanding the influences of various suspension parameters on vehicle drift, then implementing the necessary changes directly to the manufacturing process. Since the total amount of work required a timeline that exceeded a Masters program, it was divided into two dependent projects: The development of the high-fidelity full vehicle model using MSC.Adams and model correlation with physical component testing and validation with physical road testing. The latter part of the development could not be completed within my Masters program.

Thus, the goal of this research is to develop the high-fidelity full vehicle model in MSC.Adams to simulate the influences of suspension parameters on vehicle drift of the subject sports utility vehicle.

Chapter 2

Literature Review

2.1 Terminology and Coordinate Systems

2.1.1 Suspensions

The suspension links the wheels to the vehicle body and allows for relative motion between the two masses [18]. The system consists of springs, dampers, and linkages that must satisfy a number of requirements related to road handling performance and occupant comfort. Forces and moments that are present between the interaction of the tire contact patch and the ground are directed through the suspension components and into the vehicle body.

The kinematics of the suspension can be described by understanding that for any body moving in space relative to another body, its motion can be defined by three components of translation and three components of rotation [15]. In the context of independent suspensions, which allow for relative motion between the wheel and the vehicle body without affecting the opposite wheel, the wheel has only one path of motion. Like any single body

in space, the wheel has six degrees of freedom, but with five degrees of freedom restrained by linkages. Essentially, the suspension linkages severely limit the orientation of the wheel as it travels up and down against the dampers and springs, which may rotate about its three axes due to the geometry of the suspension. Ideally, a perfect suspension system would not allow such rotations during its linear up/down travel path. In the real world, such systems do not exist, but effective tuning of the suspension would offset the effect of such rotations.

The various angles associated with the rotation of the knuckle, to which the wheel attaches are known as camber, caster, and toe angle. The camber angle is the angle between the wheel to the vertical axis of the vehicle when viewed from the front or rear of the vehicle (as shown in Figure 2.1). A positive camber angle is described when the top of the wheel is farther out than the bottom. As such, a negative camber angle is described when the bottom of the wheel is farther out than the top. The toe angle is the angle that the wheel makes with the longitudinal axis of the vehicle, when the steer angle is zero (as shown in Figure 2.2). Negative toe, also known as toe out, occurs when the front of the wheel is directed outwards from the vehicle. The wheel is directed inwards for positive toe, or toe in. Unlike the other wheel angles, the caster angle cannot be measured directly from the wheels. Rather, it is the angle made between the steer axis of the wheel and the vertical axis of the vehicle (as shown in Figure 2.3). A positive caster angle is described when the steer axis is forward of the vertical axis at the intersection with the ground when viewed from the side.

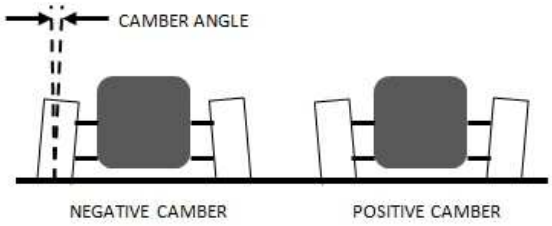

Figure 2.1: Camber angle as viewed from the front

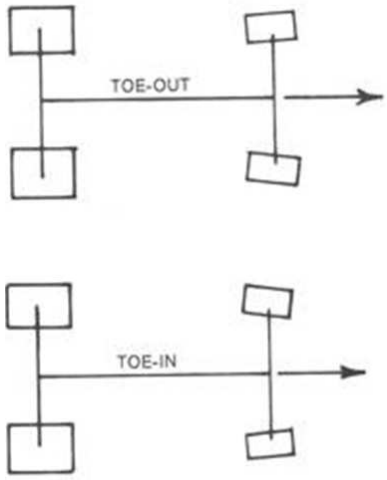

Figure 2.2: Toe angle as viewed from the top

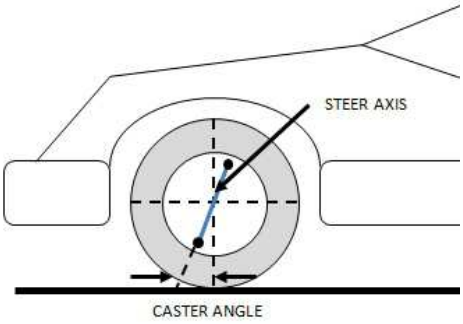

Figure 2.3: Caster angle as viewed from the side

Other components of the suspension include springs, dampers, and bushings. The role of the damper is to absorb the vibration associated with driving on uneven terrain [17]. The springs provide a force to return the wheel to its desired height when the wheel

experiences vertical displacement. The bushings, which are usually present at the joints of the suspension linkages, are compliant components of the system that help absorb vibration from the road that will not be captured by the damper. The three components work in unison to provide a comfortable ride to the passengers.

There are numerous types of suspensions, classified as independent or dependent. However, the thesis will discuss the two types that exist with our subject vehicle. Modern cars typically have a MacPherson strut suspension due to its compactness. This suspension system is typically characterized by a wishbone like lower control arm that provides both lateral and longitudinal restraint to the centre of the wheel. The hub or knuckle is connected to both the pivot of the lower control arm and rigidly to the lower mount of the spring and damper assembly. The damper acts like an infinitely long upper control arm, constraining the wheel to rotate around its axis when steering input is applied. Unfortunately, the long upper control arm tends to increase positive camber as the wheel is compressed upwards, also known as *bump*, which can decrease maximum road handling performance.

A multi-link suspension is also deployed at the rear of the particular SUV. Typically, the system consists of at least one trailing arm, guided by two or three transverse control arms. The trailing arm is connected rigidly to the wheel hub carrier, and in some cases, serves as the wheel hub carrier. The spring and damper are located on one of the transverse linkages, although their lower pivot can be positioned separately [17].

2.1.2 Pneumatic Tires

The primary source of forces and moments which provide the control and stability of the vehicle are found at the four small patches where the pneumatic tires contact the road

surface [15, 29]. The forces and moments generated by the interaction of the pneumatic tire bear the following roles:

- Support the weight of the vehicle.
- Support vertical forces from aerodynamics.
- Supply tractive, braking and cornering forces.
- Supply forces used for controlling and stabilizing the vehicle.

The automobile tire is a complex component of the vehicle assembled from a product of rubber and synthetic materials. The exact construction of each tire varies significantly with tire types. However, most modern passenger vehicle tires consists of fibers, textiles, and steel cords woven together to form the carcass. The carcass, also known as body plies, is the main part of the tire that supports the tension generated by the internal air pressure. Depending on the angle of the weave of the plies, two types of tires exists: Radial and non-radial, or bias-ply tires. The plies in a radial tire are woven perpendicular to the circumference of the tire, whereas the non-radial tires contain plies that are layered at an angle of 30 to 40 degrees from each layer. Encapsulating the carcass is the rubber tread that is designed for various terrains and temperatures. A liner is placed on the inside of the carcass to prevent air leakage.

2.1.3 Coordinate Systems

Four coordinate systems will be introduced in this thesis. One vehicle coordinate system was standardized by the Society of Automotive Engineers (SAE) in SAE J670 [25] as shown in Figure 2.4. The SAE system employs the right-hand-rule where the index finger points down as the positive z-axis.

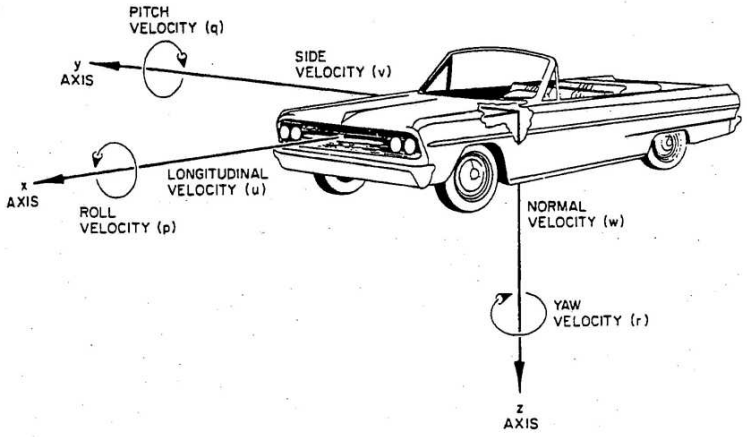

Figure 2.4: SAE vehicle coordinate system

The other coordinate system was standardized by the International Standards Organization (ISO) as shown in Figure 2.5. This is also known as the ISO tire axis system since various tire models employ this sign convention to calculate forces and moments.

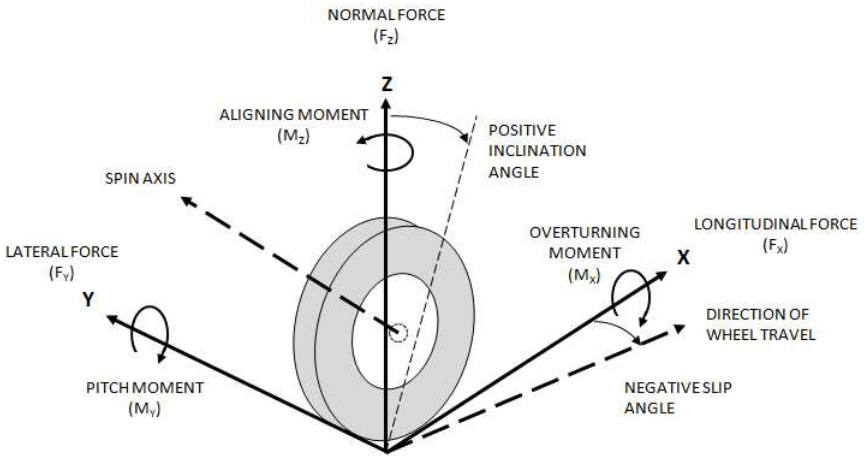

Figure 2.5: ISO coordinate system

2.2 Vehicle Drift

2.2.1 Overview

Vehicle drift is defined as the condition where the driver must apply a constant correctional torque to the steering wheel in order to maintain a straight line course. This vehicle behaviour can cause driver fatigue and discomfort, and is usually not observed in newly minted vehicles fresh off the assembly line. However, it is not unusual for auto manufacturers to design a slight drift in their vehicles to counter the effects of road crown. Road crown, as shown in Figure 2.6, is the lateral slope of a roadway, designed to aid in water drainage to prevent problems associated with hydroplaning and ice accumulation in cold weather conditions [1].

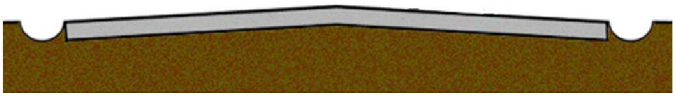

Figure 2.6: Diagram of a typical road crown

2.2.2 Vehicle Drift and Suspension Parameters

Other factors that may influence vehicle drift are well documented in the literature. Kim *et al.* [4] noted the effect of various suspension and tire parameters on vehicle drift. The results were obtained from co-simulation results of a full vehicle model constructed using Adams/Car and MATLAB. The suspension system was composed of a MacPherson strut in the front and a coupled torsion beam axle in the rear. Table 2.1 details the results from the drift simulations of the developed model driving at an unknown constant velocity. The changes to the suspension and tire parameters are left and right symmetric (i.e. Front toe of 2mm was applied to the front left and front right suspension of the full vehicle model).

Although each parameter had an effect on the drift change or lateral deviation, the sensitivity to each parameter is unknown. This is because the range of the allowable variation is unknown and is dependent on the make and model of the vehicle. Also, the nature of the experiment is not known. Therefore, it can only be gathered from the results that all suspension and tire parameters had an influence on vehicle drift.

In the paper authored by Oh *et al.* [28], various suspension and tire characteristics were analyzed with respect to vehicle drift. Results were gathered from tests performed on road going vehicles. The test method required the vehicle to maintain a constant speed of either 80 km/h or 100 km/h. The lateral movement of the vehicle was then recorded 100 metres

Table 2.1: Vehicle drift versus suspension parameters [4]

PARAMETERS	PARAMETER VARIATION	DRIFT CHANGE [m]
Front Toe	2mm	0.026
Front Camber	-0.5 deg	0.811
Front Caster Angle	0.5 deg	-0.562
Front Caster Trail	7.08 mm	1.707
Front Tire Conicity	2 kgf	0.069
	5kgf	0.172
Tire Radius	-3mm	-0.287
Rear Toe	0.2mm	0.052
Rear Camber	0.5 deg	-0.014
Rear Tire Conicity (RH)	2 kgf	0.011
	5 kgf	0.028
PRAT (4W)	1.5 Nm	0.876
PRAT (LH/RH)	-1.5 Nm	-0.857
Road Gradient	2 deg	2.083

after the release of the steering wheel.

The parameters that were tested emulated variations of manufacturing tolerances, such as cross caster and cross camber. As defined in the paper authored by Oh *et al.* [28], cross camber is the difference between the left and right camber angle (ie. his was defined in the paper as the right camber angel minus the left camber angle). Cross caster was defined similarly as cross camber.

It was found that a negative cross caster angle induced the vehicle to drift towards the

left, and a positive value induced a drift towards the right. Note that the direction of the vehicle drift is with respect to the driver's perspective.

2.2.3 Vehicle Drift and Tire Properties

In addition to the characteristics of the suspension system, tires can affect the straight line performance of a vehicle. Lindenmuth [21] showed experimentally that the conicity force of a rolling tire is directly related to vehicle pull, whereas the plysteer effects would go unnoticed in typical driving applications. Conicity is the lateral force component generated by the tire at zero slip angle mainly due to the off-centring of the top belt in a radial tire, and does not change direction with reverse rotation of the tire [26]. Plysteer is the lateral force component generated by the tire at zero slip angle mainly as a result of tire design of the plies in the belt, and changes direction with reverse rotation of the tire. Belted radial tires also generate aligning moments when rolling at zero slip angle. This behaviour is measured as the residual self-aligning moment [27].

The influence of such tire properties can be described in the following example. In order for a vehicle to travel in a straight line, the average lateral forces of the front and rear tires must be zero to achieve equilibrium. Because of manufacturing deformities, the tires on all four corners exhibit plysteer and conicity lateral forces at zero slip angle. Thus, the vehicle would be required to travel with a small side slip angle where the average lateral forces are balanced in the front and in the rear. On the other hand, it is known that tires also exhibit a self-alignment moment when the lateral forces are at zero, which when averaged in the front, tends to pull on the steering wheel. This steering pull phenomenon gives an impression to the driver that steering input is required to maintain a straight line motion [27].

2.2.4 Drift Testing

Straight line vehicle drift testing performed by the automotive industry was documented by Lee [20]. The subject vehicle was adjusted to the manufacturers specification and the test track was a flat asphalt road. The vehicle was brought up to a speed of 80 km/h and was held constant while the driver adjusted the vehicle for straight line travel. After 100 metres of adjustment, the driver released the steering wheel and the lateral deviation was measured 100 metres after the point of release. External factors such as wind speed and temperature were not recorded.

2.3 Computer Modeling

Computer modeling of multibody dynamic systems has gained increasing popularity with the engineering industry with available rising computational power. The following section will explore the simulation software that were available for use in this research.

2.3.1 CarSim

CarSim® is a vehicle dynamics simulation software developed by Mechanical Simulation Corporation in Ann Arbor, United States of America [7]. The software is based on a robust non-linear 14 degree of freedom (DOF) vehicle model that is populated by tabulated data from vehicle geometry, suspension kinematics, vehicle and component inertial properties, and forces from springs, dampers, bushings and tires. CarSim also contains programs that solve the equations of motion for vehicle models to predict motions, forces, and other variables.

2.3.2 Adams/Car

Adams®, developed by MSC Software Corporation in Ann Arbor, United States of America [12], is a Multibody Dynamics (MBD) software that is widely used in the engineering industry. The software formulates equations of motion based on absolute coordinates to obtain a time response of the system [3]. This process can be rather time consuming as complex assemblies often involve large systems of nonlinear differential algebraic equations (DAEs) requiring large amounts of computing power. Adams/Car is part of a suite of programs within Adams designed specifically for the automotive industry [13]. The program contains templates for common steering, anti-roll, and suspension systems, allowing the user to generate a vehicle model without the need to build from the ground up. An extensive library of macros is also built into the program to speed up the model creation process. Adams/Car also contains a list of related modules as listed below:

- Adams/Car Ride This module simulates the ride quality of the vehicle model by utilizing a four-post test rig model [9].
- Adams/Tire - This module can generate tire models from testing data and analyze tire data. Various tire models are supported, including Fiala and Pacejka 2002 which was slightly modified to include low speed tire characteristics for parking simulations [11].
- Adams/Smart Driver - This module contains smart algorithms to drive a vehicle to its dynamic limits or within defined targets [10].
- Adams/Car Road - This module is a *GUI* (Graphics User Interface) based program to allow the user to create 2D and 3D roads [8].

2.3.3 MapleSim

MapleSim is a MBD software developed by Maplesoft based in Waterloo, Canada [22]. Unlike Adams/Car, the program formulates equations of motion based on body fixed coordinate system. The governing equations are formulated by DynaFlexPro, which automatically creates the symbolic equations for multi-domain engineering systems based on linear graph theory [24]. This leads to more efficient systems of equations and allows for the use of symbolic equation simplification to further reduce required computational power by approximately a factor of 10 when compared to Adams [23].

2.4 Tire Models

Tires are complex engineered products and engineers have developed various complex tire models for vehicle dynamics simulations. Tire models are essentially best fit curves that approximate the characteristics of tire behaviour from physical test data [24]. It is entirely possible to model the interaction between the surface and the tires. However immense computational power is required to perform such finite element analyses [2, 5].

Before this section explores two of the more commonly used tire models in the automotive industry, the reader should be familiarized with the general characteristics of tire behaviour and its nomenclature.

As mentioned in Section 2.1.3, forces and moments are calculated by tire models in the ISO tire axis system, as shown in Figure 2.5. The ISO tire axis system is located in the centre of the *tire print* or *contact patch*, the interaction area between the tire and the road. The ISO *x-axis* lies on the tire print, the ISO *z-axis* is perpendicular to the tire print, and the ISO *y-axis* completes the right-hand rule derived coordinate system, which also lies on

the tire print. The directions of the axes are dependent on the direction of the generated tire forces. The ISO *x-axis* is parallel to the contact plane of the tire, which is also aligned along the longitudinal force F_x. When the vehicle is accelerating, the resultant longitudinal force is $F_x > 0$, and $F_x < 0$ when decelerating. The ISO *z-axis* is perpendicular to the ground plane and is parallel to the normal force F_z, also known as the wheel load. When $F_z > 0$, it is pointed upwards from the ground. Lastly, the ISO *y-axis* is pointed along the lateral force F_y.

The orientation of the tire is defined by the inclination angle (γ) and the slip angle (α). The inclination angle is not to be confused with camber angle, which is a static suspension property that is determined with respect to the front or rear view of the tire, and not according to the ISO tire axis system. The inclination angle is measured between the plane of the tire and the ISO *z-x* plane. The slip angle is the angle between the wheel velocity vector, or the direction of wheel travel, and the *x-axis*. Once again, this is not to be confused with the toe angle, as it is also a static suspension property. The angle that revolves around the *y-axis* is of no importance to tire models and analysis.

Moments acting around the centre of the tire print are also defined. The overturning moment M_x is a longitudinal moment about the *x-axis*. The pitch moment M_y is the lateral moment about the *y-axis*, and the aligning moment is an upward moment about the *z-axis*. The sign conventions of the three moments follow the right-hand rule.

With the tire orientations, and forces and moments established, basic tire behaviour can be described. To accelerate or decelerate a vehicle, longitudinal forces must be generated at the tire print. The mechanism involved in the generation of the forces will not be discussed in detail, but it is understood that an applied driving torque will create shear stresses within the tire carcass when the tread elements adhere to the road surface, which is also known as the *friction region* or *elastic region* [15]. This induces deformations within

the region of the tire print and generates a longitudinal slip, which is not analogous to the definition of the slip angle. This longitudinal slip is a measure of the difference between the rotational speed of the wheel and the translational velocity of the wheel centre [30]. Lateral force is generated in a similar fashion where an applied torque around the *z-axis* results in the widening of the slip angle, forcing the tire to track a path that is different than its heading, which is along the velocity vector. This induces shear stresses within the tire and results in the generation of a lateral force.

Tires also exhibit an aligning moment, which is described as a tires tendency to steer about a vertical axis through the centre of the tire print [25]. This is also known as the self-alignment moment, since at low slip angles the tire tends to align its heading with its travel path. In other words, tires like to point to where they are traveling. The aligning moment is a function of the pneumatic trail, which is the distance between the centre of the tire print to where the centre of the lateral force is located. This can be confusing as it is generally understood that all tire forces are generated at the centre of the tire print. This is not true, as the elasticity of the tire carcass and tread deform with shear stress, which is not uniformly distributed along the tire print.

Other characteristics common to most pneumatic passenger vehicle tires are listed in the following:

- At low slip angles, the lateral force F_y is linearly proportional to the slip angle.
- At low longitudinal slip, the longitudinal force F_y is linearly proportional to longitudinal slip.
- At high slip angles and longitudinal slip, the tire is unable to maintain maximum traction and tends to drop its lateral and longitudinal tractive capabilities.

- Tire forces increase non-linearly with the normal force.
- Due to manufacturing tolerances, all tires exhibit lateral forces and an aligning moment at zero slip angle. The forces were previously described in Section 2.2.3 as conicity and ply steer. Plots illustrating this phenomenon are shown as Figure 2.7 and Figure 2.8.
- A negative inclination angle generally induces higher lateral forces. This additional lateral force is referred to as *camber thrust* and tends to fall off at camber angles above 5° [15].

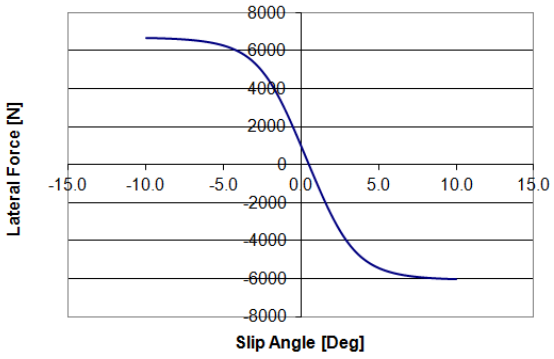

Figure 2.7: Exemplar lateral forces at zero slip angle

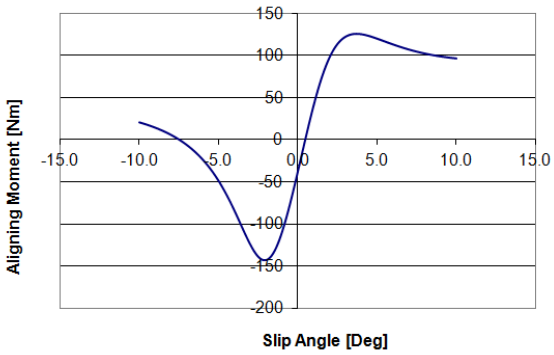

Figure 2.8: Exemplar aligning moment at zero slip angle

2.4.1 The Fiala Tire Model

The Fiala tire model was first introduced in 1954 and is based on 6 parameters which are directly related to the physical properties of the tire. This basic tire model was further

extended by Adams/Car in their 2005 software release [14]. Though the model is computationally friendly, it has certain limitations when compared to other existing empirically derived tire models. The following lists the limitations and assumptions:

- The tire print is always rectangular.
- Camber thrust is ignored assuming the inclination angle has no effect on tire forces.
- Forces and moments at zero slip angle are always zero, thus eliminating ply steer, conicity and aligning moment at zero slip.
- Lateral and longitudinal tire stiffness does not vary with normal load [24].
- Combined longitudinal and lateral slip is not accurately represented.

As a result, this model was deemed to be ineffective.

2.4.2 The PAC2002 Tire Model

The PAC2002 tire model was developed by Adams/Car and is based on the Magic Formula Tire model, first introduced by Pacejka [26]. The model is considered to be extremely accurate for describing tire behaviour for smooth roads and is used extensively in the automotive industry. Unlike the Fiala tire model, the PAC2002 tire model accounts for camber thrust, non-zero forces and moments at zero slip angle, varying lateral and longitudinal tire stiffness with normal load, and can also represent combined lateral and longitudinal slip.

The formulation of the model is based on a trigonometric curve fit with six coefficients: B, C, D, E, S_h, and S_v. The following equations are the basis of the PAC2002 tire model:

$$y(x) = D\cos[C\arctan\{Bx - \arctan(Bx)\}] \tag{2.1}$$

$$x = X + S_h \tag{2.2}$$

$$Y(X) = y(x) + S_v \tag{2.3}$$

Where $Y(X)$ are the forces or moment to be determined ($F_x, F_y, or M_z$) as a function of X, which can be longitudinal slip (γ) or slip angle (α). The variables y and x are intermediate variables to account for the vertical offset S_v and horizontal offset S_h of the curves.

The coefficients B, C, D and E define the shape of the curve [11]:

- D determines the peak of the curve.
- C influences the shape of the curve.
- B stretches the curve, affecting the stiffness of the characteristic.
- E modifies the curvature of the peak.

The coefficients are calculated by equations proposed by Pacejka that utilize an extensive list of parameters related to the tires properties. These equations and parameters are too lengthy to be presented in this thesis.

Chapter 3

Tire Verification Models

3.1 Overview

Two types of models were created to test and verify the behaviour of the generated PAC2002 tire models as described in Section 2.4. One model is described as the *tire test-rig model*, which is essentially a 1-DoF model attached to one tire. This model was used to compare the PAC2002 tire models as simulated in Adams 2010 and MapleSim 5 to calculate values from a custom tire property spreadsheet. However, inclination angle was set to zero and both plysteer and conicity forces were reduced to zero at zero slip angle, in order to simplify the test. The other model is labeled as the 6/7-DoF Vehicle Model and is composed of a fully dimensioned vehicle frame with 4 attached tires. The tires are attached to a joint that allows for variance in the tires inclination angle. Unlike the 1-DoF model described above, this model includes a tire model with the plysteer and conicity forces allowing the model to verify the effect of the residual lateral tire forces.

3.2 Tire Test-Rig Model

This model was first created in Adams 2010 then emulated in MapleSim. It is known that the PAC2002 model contains more than 100 parameters and is quite complex in nature, and thus a sensitive test such as vehicle drift testing could be fairly susceptible to small variations. Since the tire models were generated with a customized spreadsheet, confidence in the emulated model's residual tire lateral forces can be confirmed by creating similar test-rigs in two different multi-body software packages. The simulation results can then be compared to the spreadsheet calculated values, which should be quite similar given the same initial conditions.

3.2.1 Adams Tire Test-Rig Model

The tire-test rig model consists of one tire that is connected to a rigid link with an idealized revolute joint. The rigid link is then connected to the ground through a "restricted" planar joint. This planar joint allows a plane on one part to slide in the plane of another part, but restrict all rotations. In other words, the tire is allowed to roll along the ground but is not allowed to rotate about its steer axis, limiting the model to three degrees of freedom (i.e. two translations along the ground plane and rotation about the rotational axis of the wheel). This is done to prevent any undamped oscillations about the steer axis and to isolate the effect of the tire residual lateral forces. To generate the correct amount of normal forces as experienced on the SUV, the length of the rigid link was calculated from the tire vertical stiffness ($C_z = 21000N/m$) to apply a normal force equal to half of the front corner weight, which was approximately 6100 Newtons. Also, the wheel orientations were set to neutral: Camber, caster and toe angles were given a value of zero. The PAC2002 model of the Bridgestone Dueler H/L 400 all-season tire was used for the simulations. However, the

parameters were altered to reduce the total plysteer and conicity forces to be negligible (i.e. zero forces at zero slip angle). Since the camber angle or inclination angle was set to zero, the tires lateral force sensitivity parameter to camber angle was left untouched. The model as designed in Adams 2010 is shown in Figure 3.1.

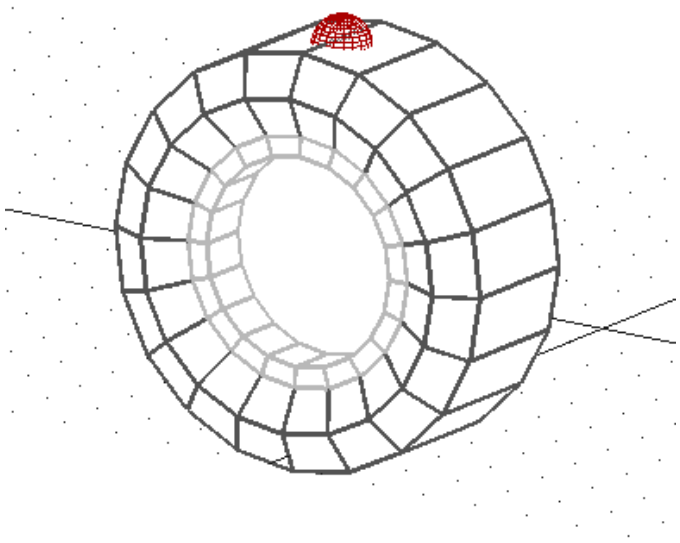

Figure 3.1: Tire test-rig as modeled in Adams 2010

Preliminary simulation results indicated that the tire-rig assembly was unstable at the start of the simulation due to the unrestricted planar translations. Thus, a sinusoidal lateral prescribed motion was introduced in the form of Equation 3.1 with a constant longitudinal velocity of 100 km/h for 5 seconds. The prescribed motion alters the model to have only one degree of freedom. Instead of comparing the lateral drift over the 100 metres of distance, the peak lateral forces and lateral slips were used for verification.

$$y(t) = 250sin(time) \tag{3.1}$$

3.2.2 MapleSim Tire Test-Rig Model

The MapleSim tire test-rig was modeled in the same fashion as the Adams 2010 model. A diagram of the vehicle model is illustrated as Figure 3.2.

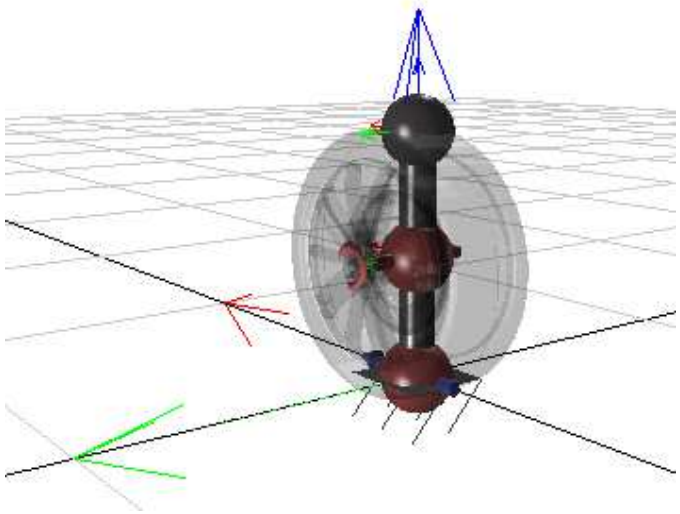

Figure 3.2: Tire test-rig as modeled in MapleSim 5

3.2.3 Simulation Results

To have a fair comparison of the simulation results from the MapleSim and Adams 2010 models, ideally, a fixed step solver would be employed. However, the only solver available at the time of writing that was identical in the two software packages was the variable time

step Runge-Kutta 4/5, which is a method for numerical solution of ordinary differential equations. The simulations were solved using an initial time step of 10^{-5} seconds. It was found that the peak lateral slip and lateral tire forces were very similar between the two programs, as shown in the Figure 3.3 and Figure 3.4. Note that the two curves in the two graphs were overlaid on top of each other.

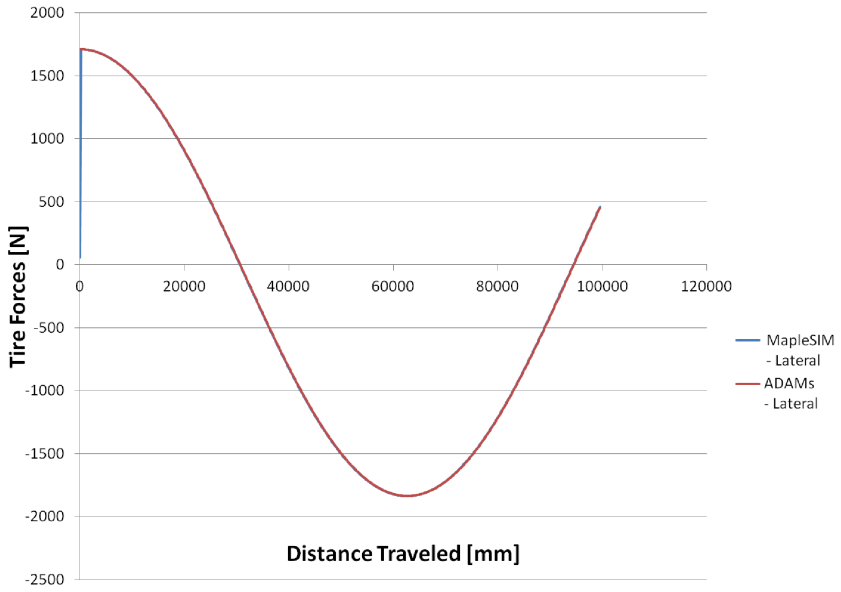

Figure 3.3: Tire lateral forces - Adams and MapleSim

However, as shown in Figure 3.5, the MapleSim results had a blip at the start of the simulation. This phenomenon is explained as initial transients that were not handled by MapleSim, unlike Adams 2010 which had built-in functions to first settle the model before running the full simulation. This allowed the initial transients to settle themselves so that the simulation would begin at equilibrium.

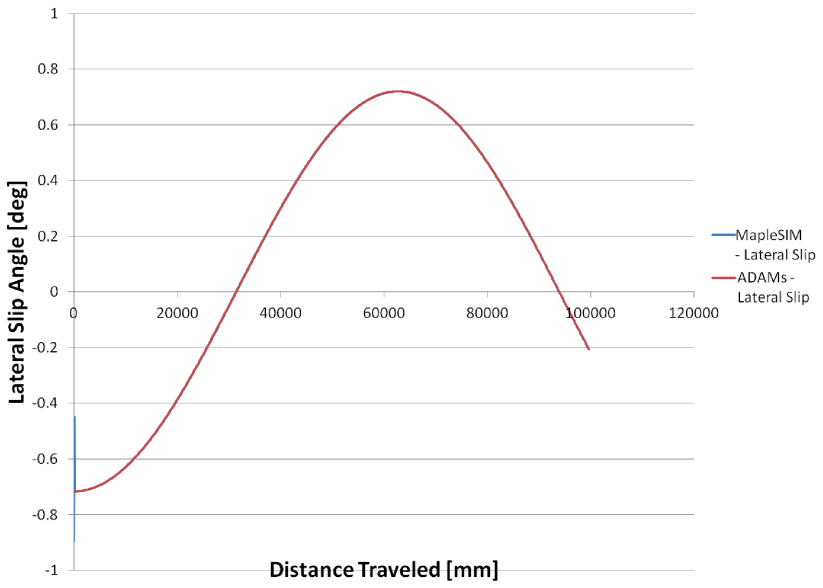

Figure 3.4: Tire lateral slip angles - Adams

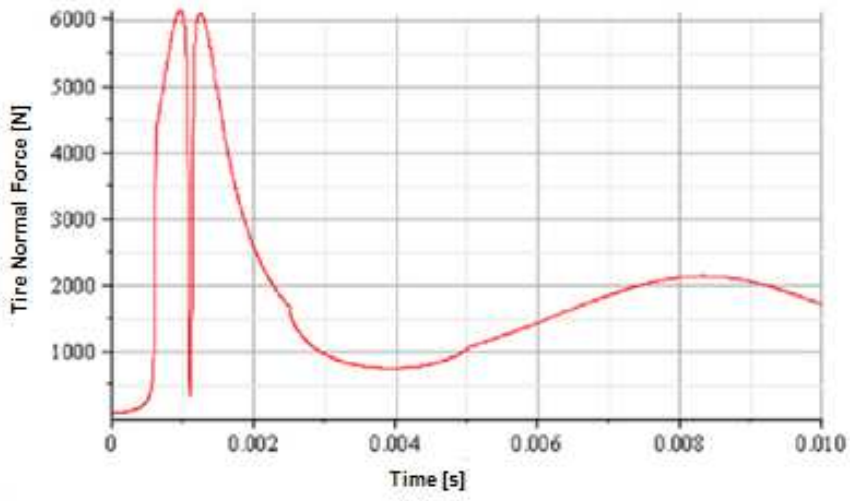

Figure 3.5: Tire lateral forces - MapleSim

A custom spreadsheet based on the PAC2002 tire model formulation was created to generate the tire models. This spreadsheet was designed in Microsoft Excel to make use of its ability to conveniently track the required large amount of tire property parameters. The **goal seek** function contained within the software was utilized to vary parameters $pHy1$ and $pVy1$ to obtain the specified lateral force at zero lateral slip, while maintaining other tire properties constant (i.e. cornering stiffness, cornering force, and aligning moment at one degree of slip angle as specified by the OEM). Parameter $pHy1$ was varied as it was mainly responsible for the horizontal shift of the lateral force curve, and likewise, $pVy1$ was responsible for the vertical shift of the lateral force curve.

When compared with the spreadsheet calculations, the peak lateral force at the maximum lateral slip angle was very similar. Difference between the simulated lateral force and the calculated lateral force was less than 1.5%. Table 3.1 shown below describes the values obtained. Note that the high lateral forces exhibited by the MapleSim tire-test rig model during the first 0.010 seconds were ignored for this comparison.

Table 3.1: Peak lateral forces.

	Spreadsheet	**MapleSim**	**Adams 2010**
Normal Force [N]	6100	6100	6100
Lateral Force [N]	1685	1700	1710
Lateral Slip Angle [Deg]	-0.72	-0.72	-0.72

3.2.4 Conclusion

Two models created in MapleSim and Adams 2010 are identical in design and nature. The tire parameters were based on an existing model, but were altered to accommodate the tire

properties of the Bridgestone Dueler H/L 400 all-season passenger tire. The simulation results indicate that the peak lateral slip and lateral tire forces were very similar between the two programs used. It was found that a small blip at the beginning of the simulation for the MapleSim program was attributed to initial transients that the software was unable to settle before the start of the simulation. As such, not only did the tire behave as expected on the tire test-rig model, but the peak lateral forces simulated by Adams 2010 and Maplesim 5 only differed by 1.5% from the values calculated by the custom PAC2002 tire model spreadsheet. Thus, the results add confidence to the usage of the PAC2002 tire model for the full-vehicle model.

3.3 6/7-DoF Vehicle Model

This model was also created in Adams 2010 then emulated in MapleSim. The main purpose of this model is to test and verify the effect of the tires residual lateral forces once there was ample confidence in the generated tire model. Recall that the results from the 1-DoF tire test-rig model from Section 3.2.3 indicated that the tire model was shown to have similar lateral forces between the Adams 2010 and MapleSim, and also from the calculated tire forces generated from PAC2002 equations. A conclusion can then be drawn from a straight-line drift test, from which the results will be compared between the two multi-body solvers and to a theoretical calculation of drift. Two variations of the base model were created to understand the effects of tire lateral forces on vehicle drift, the 6-DoF and 7-DoF vehicle models. Four of the six/seven degrees of freedom were represented by the rotation of the four wheels. As the entire chassis is attached to the ground via a planar joint, the vehicle is allowed to freely translate and rotate along the ground plane. The 7-DoF model allows for free planar translation and rotation about the *z-axis*, whereas the

6-DoF model only allows for free planar translation with no yaw. Also, steering is not active in this model, and is left locked at zero steer angle.

3.3.1 Adams 6/7-DoF Vehicle Model

The model created in Adams 2010 consists of four tires attached to the frame of the vehicle. The frame was designed with the same dimensions as the subject SUV so that the four tires are located at their corresponding wheel centre locations. The entire frame is fixed in height to the ground via a rigid link that is attached to a planar joint connected to the ground plane. The vehicle frame then extends to each corner where an *upright link* can be adjusted to give the appropriate amount of compression to generate the normal forces similar to the subject vehicle. Though the mass of the chassis does not have a direct effect on the normal forces applied at the wheels, the correct mass was modeled according to the vehicle's nominal specification to maintain the correct inertial property. At the wheel, a revolute joint allows for changes to the constant camber angle (refer to Figure 3.6 and Figure 3.7).

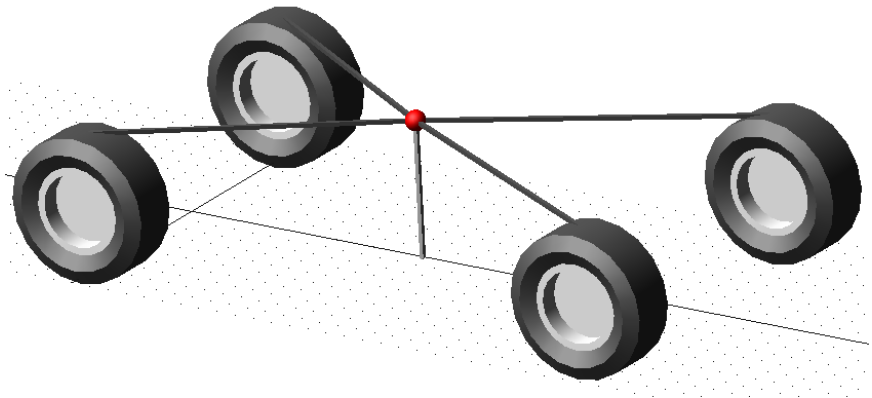

Figure 3.6: The 6/7-DoF vehicle model in Adams 2010

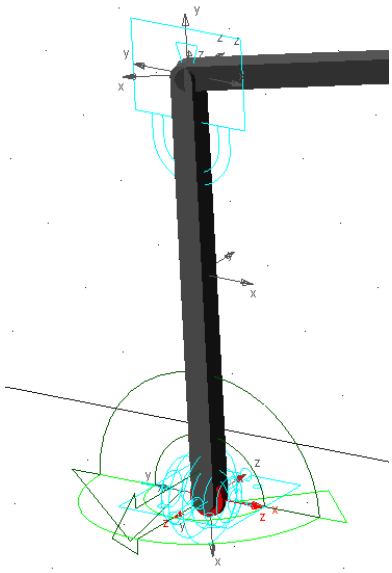

Figure 3.7: The customized joint for the 6/7-DoF vehicle model.

3.3.2 MapleSim 6-DoF/7-DoF Vehicle Model

The MapleSim 6-DoF/7-DoF was modeled in the same fashion as the Adams 2010 model. A diagram of the vehicle model is illustrated as Figure 3.8.

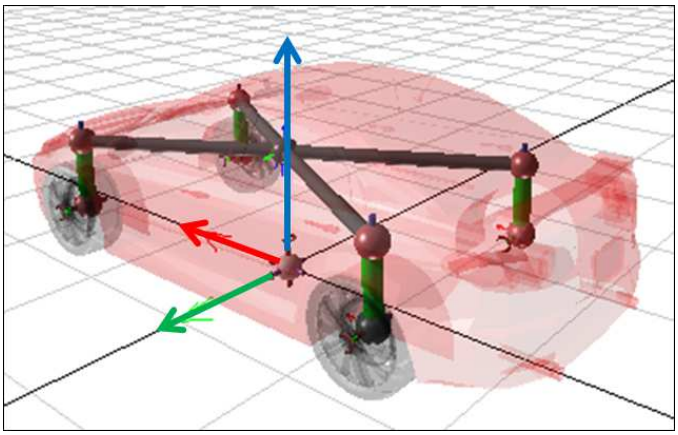

Figure 3.8: The 6/7-DoF vehicle model in MapleSim

3.3.3 Simulation Resuts

To have a fair comparison between the two multi-body solvers, the Runge-Kutta 4/5 method was employed to numerically solve the differential equations generated by the models. The camber angle was set to be -0.67 degrees at all four corners. The normal force generated in the front tires was approximately 6100 Newtons, and the rear tires experienced approximately 4800 Newtons. The total residual tire lateral forces at the pre-determined camber angle were set to be 60 Newtons of force as computed by the custom tire model spreadsheet based on the PAC2002 equations as described previously.

All simulations were run with the models having an initial velocity of 20 metres per second. The models were allowed to travel along a flat terrain for approximately five seconds, sufficient to cover more than 100 metres longitudinally. Recall that the Adams solvers incorporate algorithms to settle the model given initial conditions, whereas the MapleSim model does not. As such, it was expected that there would be discrepancies with the two simulations.

The simulation results from the 6-DoF model indicate that there was an excellent agreement between the MapleSim and Adams models. Individual tire lateral forces were applied to the vehicle roughly 60N towards the right (i.e. as viewed from on top), consistent through its travel. At 100 metres, the Adams model drifted 40.81 millimetres to the right, and the MapleSim model drifted 40.79 millimetres to the right as well. The slight difference was attributed to the settling algorithm present in the Adams model. The tire normal forces of the two simulations are shown as Figure 3.9 and Figure 3.10. Likewise, the tire lateral slip angles are shown as Figure 3.11 and Figure 3.12.

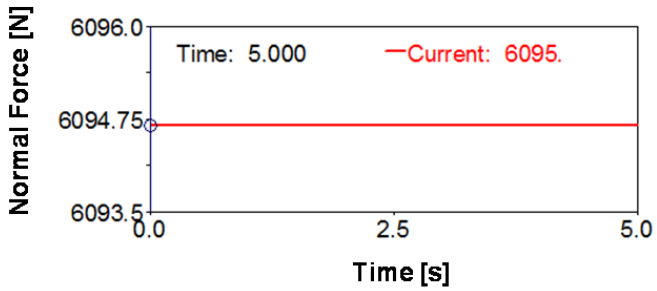

Figure 3.9: Tire normal forces - Adams 6-DoF simulations

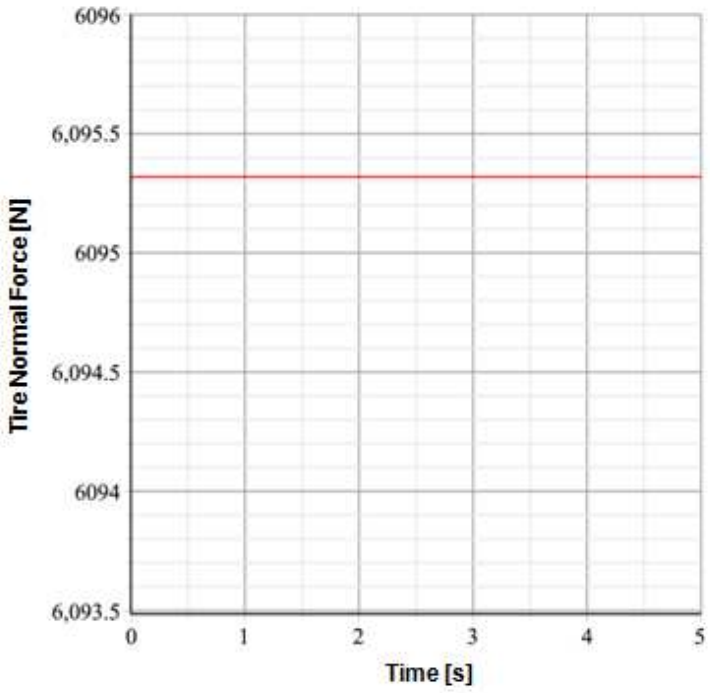

Figure 3.10: Tire normal forces - MapleSim 6-DoF simulations

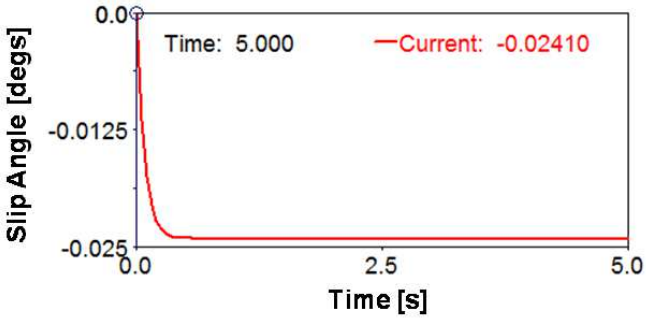

Figure 3.11: Tire lateral slip angle - Adams 6-DoF simulations

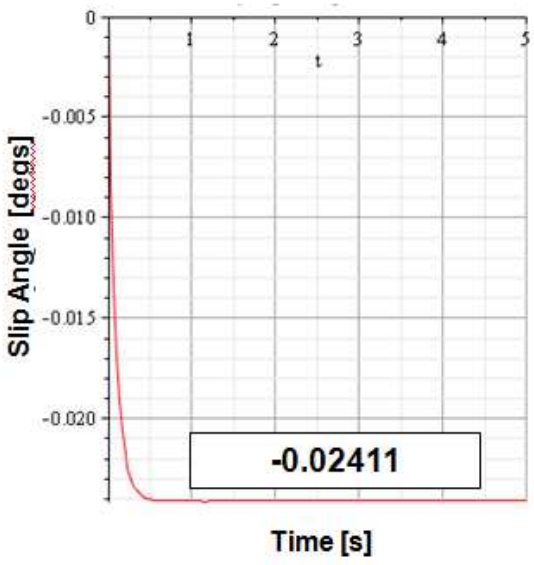

Figure 3.12: Tire lateral slip angle - MapleSim 6-DoF simulations.

The simulation results from the 7-DoF model exemplified the expected discrepancies. The total drift of the Adams 7-DoF model was 35.96 millimetres to the right over 100 metres, whereas the MapleSim model drifted 38.63 millimetres to the right. The tire lateral slip and vehicle yaw rate were compared (as shown in Figures 3.13, 3.14, 3.15, and 3.16). The tire lateral forces were similar between the two models, which was approximately 60 Newtons at the beginning of the simulation and reached zero upon achieving steady state. This is not surprising as the model is trying to attain a steady yaw rate to offset the applied tire lateral forces. In doing so, the achieved yaw rate naturally reduces the tire lateral forces to roughly zero. Similarly, the lateral slip angles between the two solvers were identical and reached a steady value approximately -0.024 degrees of towards the end of the simulation.

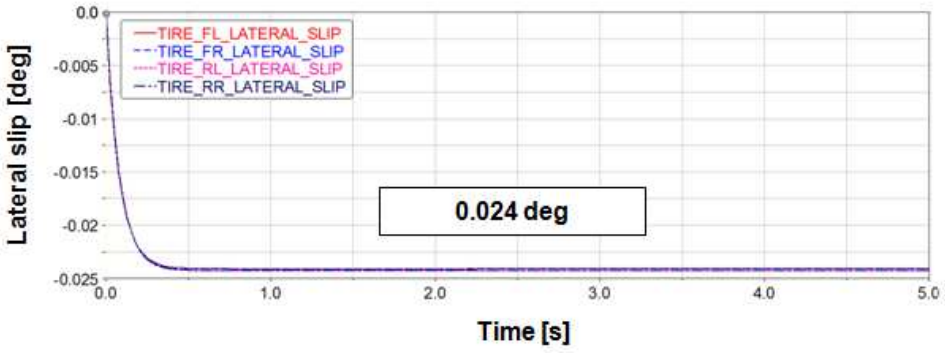

Figure 3.13: Tire lateral slip angle - Adams 7-DoF simulations

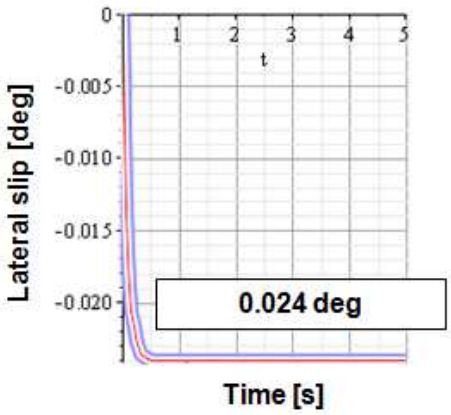

Figure 3.14: Tire lateral slip angle - MapleSim 7-DoF simulations.

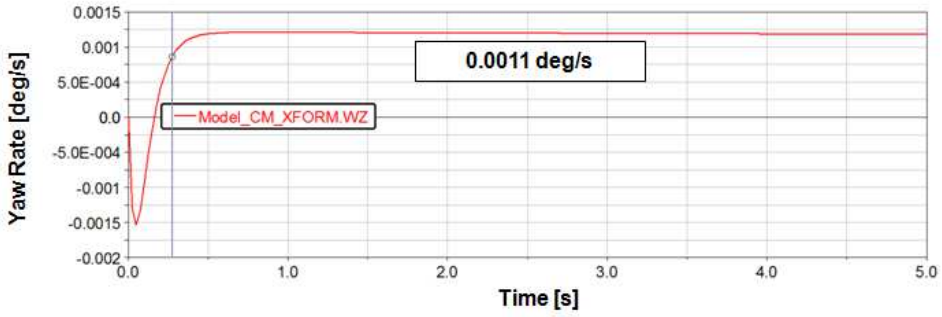

Figure 3.15: Vehicle yaw rate from - Adams 7-DoF simulations.

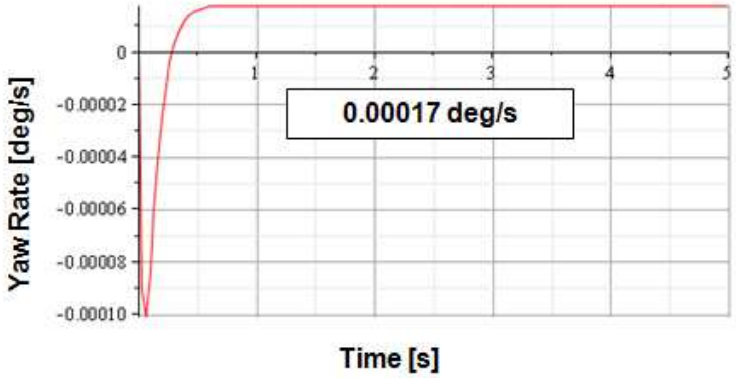

Figure 3.16: Vehicle yaw rate - MapleSim 7-DoF simulations.

The difference in drift between the two 7-DoF models was attributed to the difference in the steady yaw rate. For the Adams model, it achieved a steady yaw rate of 0.0011 degrees per second, whereas the MapleSim model achieved a steady yaw rate of 0.00017 degrees per second. Once again, the settling algorithms present in the Adams solvers likely dampened the model at the initial onset of the simulation and altered the initial conditions.

To further confirm the difference in drift, a convergence study was performed on the models. The initial time steps and error were varied from 50 to 1000 and 1.0^{-3} and 1.0^{-5}

respectively. It was found that the lateral displacement or drift was not affected by the variance in solver parameters.

Another test was performed to understand the difference in drift. The road friction was varied from 0.5 to 1.0. It was found that a direct correlation can be made between the vehicle drift and the road friction in the Adams 7-DoF model: Increasing the road friction decreased the vehicle drift, as shown in Figure 3.17.

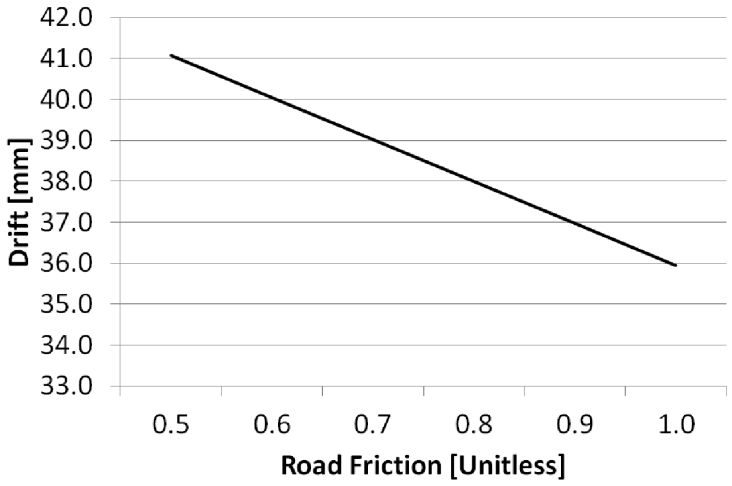

Figure 3.17: Road friction study results simulated using the Adams 7-DoF model.

3.3.4 Summary

Once again, recall that the models created in MapleSim and Adams 2010 are identical in design and nature. Locking the models yaw resulted in a vehicle lateral drift that was comparable between the two models. With the forward velocity constant, the total drift can be calculated knowing the time required to travel 100 metres longitudinally. The final calculation equates to 702 millmetres, which is much larger than the simulated results. It

is likely that there are other interaction forces between the ground and tires at play, but it is outside the scope of this document.

Nonetheless, the simulations demonstrated that the tire lateral forces modeled in both Adams and MapleSim pulled the vehicle in the correct orientation. The results also illustrated that the tire lateral forces induce a yaw rate to the vehicle, until a steady rate is achieved when the tire lateral forces approaches zero. The conclusions drawn from the results allow for confident usage of the PAC2002 tire models for the high fidelity full vehicle model.

Chapter 4

Full-Vehicle High Fidelity Model Created in Adams

4.1 Overview

It must be stated that the purpose of this research was to create a high-fidelity full-vehicle model, but it was apparent that the full list of required parameters could not be obtained from the OEM directly. Thus, certain vehicle parameters were estimated using various methods, as described in the following sections. However, a significant amount of effort was directed at developing a model platform from the ground up that would be tuned once accurate data was obtained from physical testing in the next phase of this project [19].

The vehicle that was modeled is a road-going sports utility vehicle (referred as the 'SUV' within this thesis) that was released to the public market after a redesign from the previous generation. The new generation vehicle replaced the previous MacPherson strut rear suspension with a semi-trailing arm multi-link suspension, but kept the front

MacPherson strut suspension. Also, the previous belt-driven hydraulic rack and pinion steering system was replaced with an electric rack and pinion power steering (EPS) system. The vehicle was configured with front wheel drive only.

Adams/Car was chosen as the MBD software for this research for its ability to develop a full-vehicle high fidelity model without the need for physical test data. Unlike CarSim, vehicles in Adams/Car can be modeled by defining the rigid bodies, joints, force elements, and applied motions. The rigid bodies, such as suspension linkages, wheels and vehicle chassis components, are defined by its type, mass, centre of mass (CoM), inertial properties, and joint connection locations and orientations. Motion between the rigid bodies is modeled by joints, such as bearings and balljoints, which control the degrees of freedom between the attached bodies. In Adams/Car, there is an option to switch between **kinematic** and **compliant** modes for simulation purposes. Kinematic mode forces the model to turn off compliant joints and rely on ideal kinematic joints. Likewise, compliant mode forces the model to turn off the kinematic joints and rely on compliant components like bushings. Force elements represent the forces generated by springs, dampers, bushings and tires, which are defined by mathematical functions. They act on the rigid bodies, and so their locations must be defined as well. Lastly, the applied motions, such as road surfaces and four-post test rig actuators, provide excitation to the model.

The Adams/Car model topology is based on a hierarchical database of sub-assemblies and components. At the top, an *assembly* is defined by a compilation of *subsystems* and an assembly file containing vehicle parameters, such as camber, toe, brake ratio, frontal aerodynamic area etc. These subsystems are based on standard Adams/Car templates, which are parametric models built by expert users that define the default geometric data and topology of models [8]. To generate a subsystem, a subsystem file is required that supplies the template with sub-assembly level parameters such as hardpoints, spring rates,

inertial properties, dampening ratios etc. The subsystems are adhered together with the use of *communicators*. Communicators are elements that enable the exchange of information between subsystems, templates, and other external systems such as test rigs. These elements can either specify a location on a subsystem to be joined to another subsystem, or they can specify a parametric value that can be passed from one subsystem to another, or to an assembly. For example, from the assembly level the user can specify the front camber angle, which is passed down to the front suspension subsystem that will alter the orientation of the upright to achieve the required angle. Essentially, the database of an assembly consists of text files containing parametric values that are linked to a subsystem template.

The full-vehicle model was created from standard Adams/Car templates with minor modification. Table 4.1 summarizes the standard templates that were used.

Table 4.1: Sub-assembly templates in Adams/Car.

Subsystem Name	Adams/Car Standard Subsystem Template
Front MacPherson Suspension	macpherson.tpl
Rear Multi-link Suspension	multi_link.tpl
Rack and Pinion Steering	rack_pinion_steering.tpl
Chassis	rigid_chassis_lt.tpl
Front Anti-Roll Bar	antiroll_simple.tpl
Rear Anti-Roll Bar	antiroll_simple.tpl

The vehicle model was first created by determining the locations and orientations of the rigid bodies and joints. These locations are known as *hardpoints* and were mostly

obtained from component and assembly drawings supplied by the OEM. Hardpoints that were not found in the component and assembly drawings had to be calculated from multiple drawings in order to obtain the location in 3D coordinates.

The joints connecting the rigid bodies are modeled based on their physical representation. However, not all rigid bodies are kinematically constrained. Rather, bushings are often used to attach suspension components to satisfy the designer's need to improve the ride characteristics of a vehicle. Bushings are characterized by stiffness and orientation in all three axes. However, the bushing damping rates were not provided, and thus the default values were estimated as 1% of the linear stiffness rates [16].

Inertial properties of the vehicle system and its components are vital to yield accurate simulation results. Although static vehicle simulations are mostly sensitive to the mass properties, the moments of inertia of the vehicle components are required for dynamic simulations. Ideally, these properties would be supplied, but only the masses of the components were available from the component drawings. Alternatively, the data can be obtained by physically measuring each component, but this can be tedious and impractical due to the sheer number of components. Instead, the moments of inertia, as well as the locations of the centre of mass (CoM) were largely estimated by Adams/Car given a rough geometry and material properties of the components. However, because Adams/Car is unable to model complex shapes, a small majority of the component's inertia are slightly under or over estimated. Fortunately, the nature of vehicle drift testing would not warrant the need for accurate moments of inertia as the vehicle is not subject to any significant dynamic loading during the physical straight-line testing and its representative simulation modeled in Adams/Car.

Due to the confidential nature of the vehicle's data, the values are not presented in this thesis.

The following sections will illustrate in detail the methodology that developed this Adam/Car full-vehicle from the ground up. Also, modeling techniques specific to this model and quality checks of the model will be discussed.

4.2 Modeling Coordinate System

Two coordinate systems were present during the modeling process. The coordinate system used by the OEM's engineers differed slightly from the coordinate system utilized in the Adams/Car modeling environment. The OEM's X-Y plane is placed under the ground, whereas the Adams/Car X-Y plane is located at ground level. This is likely because the engineers designed the vehicle with multiple combinations of wheel sizes, and used an offset for each variance. The location and directions of the other axis remained the same, as shown in Figure 4.1 and Figure 4.2.

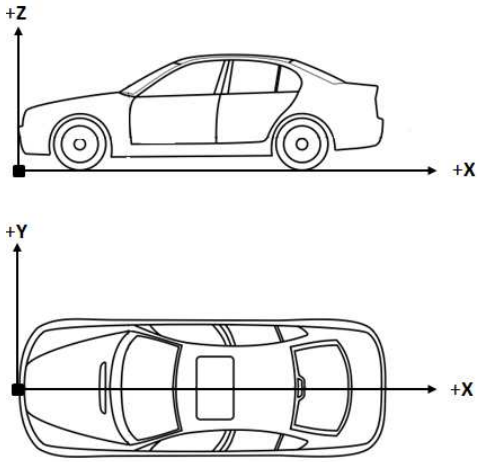

Figure 4.1: Adams/Car modeling coordinate system

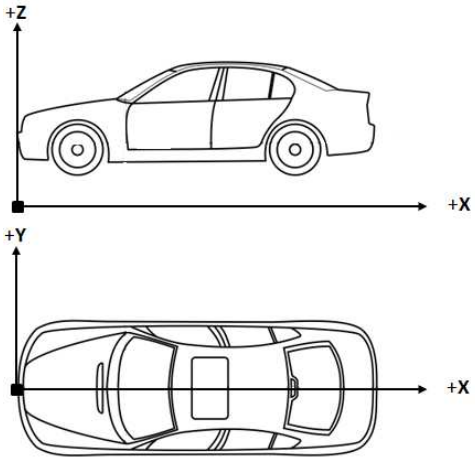

Figure 4.2: OEM modeling coordinate system

4.3 Vehicle Systems and Components

This section will explore the methodology of developing the full-vehicle model of the SUV from the ground up by detailing the following vehicle systems and components: Front and rear suspension system (including bushings, springs, dampers, and anti-roll bars), steering system, chassis, and tires.

4.3.1 Full-Vehicle Parameters

To generate the full-vehicle, a few parameters were determined. The vehicle curb weight was used to calculate the vehicle mass. The weight distribution and the location of the centre of gravity of the vehicle could not be set by the model as Adams/Car computes this based on the weight of each component included in the assembly. Rather, the centre of mass of the chassis component was specified in order to satisfy the full-vehicle values. The suspension geometry can also be modified at the assembly level of the model. The camber and the toe angles of the front and rear suspension models are decoupled from the physical hardpoints of the suspension.

4.3.2 Front Suspension System

The front suspension of the SUV is a derivation of the Macpherson strut suspension found in the previous generation of the vehicle. The system consists of a damper and spring assembly attaching the upright to the front chassis subframe. A lower control arm joins the upright to the chassis subframe and the tie-rod connects the upright to the rack and pinion steering rack. A front stabilizer bar is attached to the front subframe with bushings

and acts between the left and right lower control arm. Figure 4.3 illustrates the front right suspension of the subject vehicle as modeled in Adams/Car.

The lower half of the damper is attached rigidly to the upright, whereas the upper half is attached to an upper damper bushing. The lower control arm is joined to the upright by a lower ball joint that is modeled as a spherical joint. Two bushings attach the lower control arm to the chassis front subframe and are oriented according to drawing specifications. The upright is connected to the tie-rod via another spherical joint.

Slight modifications to the standard Macpherson strut suspension template were required to fit the SUV's suspension. The modification is listed as follows:

- The orientation of the lower control arm rear bushing was flipped.
- The lower half of the damper is rigidly attached to the upright, whereas a revolute joint was present in the original template.
- The coil springs line of action, the imaginary line where the spring force acts through, is not collinear with the dampers central axis. To accomplish this, the upper and lower hardpoints of the spring seat were altered.

The spring stiffness was dialed into the model as a linear curve, but the front shock absorbers were modeled with a non-linear curve. All bushings were modeled based on their orientations, translational and rotational stiffness. The orientation of the bushings is particularly important as the SUV's front suspension was designed with bushings arranged different than the standard Adams/Car MacPherson suspension template.

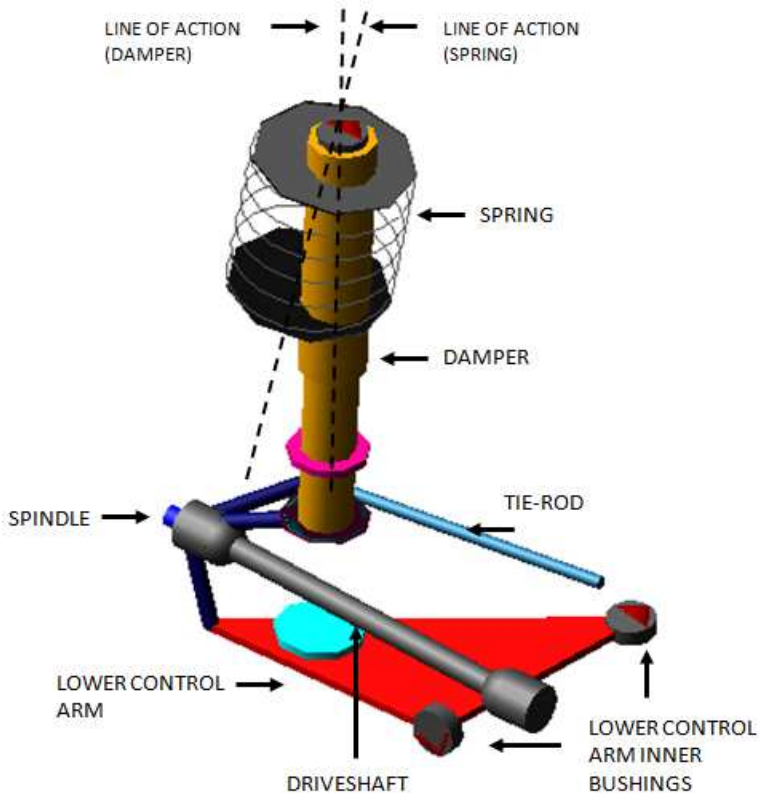

Figure 4.3: Macpherson strut front suspension - Right side

4.3.3 Rear Suspension System

The multi-link rear suspension of the SUV replaces the previous MacPherson strut design for improved handling and greater cargo space. The system consists of multiple links attaching the spindle to the chassis, and a particular spring and damper system. The damper attaches to the chassis and the spindle, whereas the spring rests between the rear subframe and the *rear lateral suspension link*. An *upper suspension link* attaches the top of the spindle to the chassis, and a *track rod* suspension link connects the front of the

spindle to the chassis. The rear suspension also includes a longitudinally aligned *trailing link*. Figure 4.4 illustrates the modeled rear suspension.

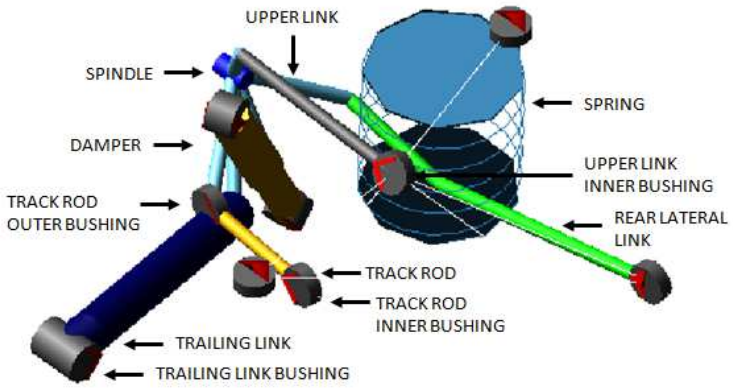

Figure 4.4: Multi-link rear suspension - Right side.

The lower half of the damper attaches to the spindle via a bushing, and similarly, the upper half attaches to an upper damper bushing. The rear lateral link connects to the chassis via a bushing, and also attaches the spindle with a ball joint that is modeled as a spherical joint. The upper link attachment to the chassis is similar to that of the rear lateral link. The track rod attaches to the chassis and the spindle with bushings. Finally, the trailing link attaches the spindle rigidly, but with a bushing to the chassis.

Slight modifications to the standard multi-link rear suspension template were required to fit the SUV's suspension. The modification is listed as follows:

- The rear lateral link bushing that attaches to the spindle was replaced with a spherical ball joint.
- The upper control arm was replaced by a single link. The outer bushing was replaced with a spherical ball joint.

- The bushing that attaches the trailing link to the spindle was replaced with a rigid connection.
- The damper and spring locations are no longer coincident. The damper attaches between the spindle and the chassis, whereas the spring attaches between the rear lateral link and the chassis.

Like the front MacPherson strut suspension, the spring stiffness is linear, and the shock absorbers were modeled with a non-linear curve. Also, the bushings were fully modeled to incorporate translation and rotational stiffness.

4.3.4 Steering System

The steering system is based on the standard rack and pinion steering system template found in Adams/Car. The steering wheel connects to the upper column with a cylindrical joint. The upper column then attaches to the intermediate shaft with a hooke joint, which then attaches to the steering shaft via another hooke joint. The pinion is driven by the steering shaft, which in turn drives the steering rack.

The torsion bar of the steering system was modeled by a bushing. Since the full-vehicle model will not include a driver model, the properties of the torsion bar are not important and were given default stiffness and damping values. A friction element was introduced to the translational joint in the steering rack to capture the stiction and the sliding friction of the system (refer to Table 4.2).

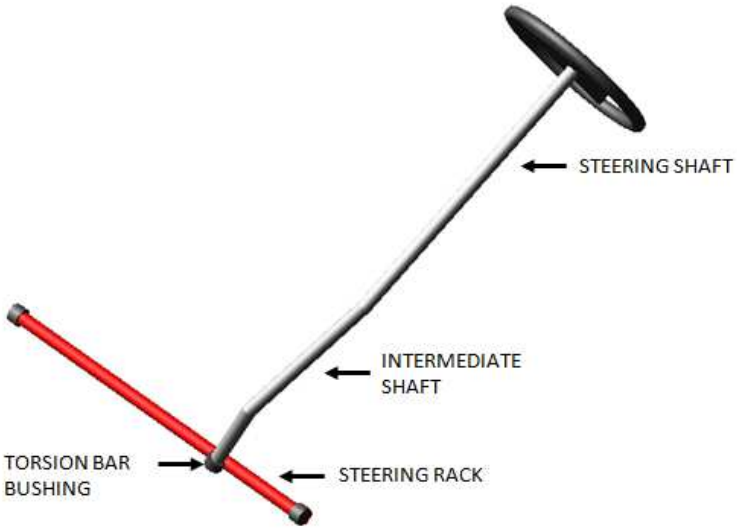

Figure 4.5: Steering system as modeled in Adams/Car

4.3.5 Wheels and Tires

The PAC2002 tire model was chosen over the Fiala tire model because it was able to account for lateral tire residual forces. According to the reviewed published literature, lateral tire residual forces have a significant contribution to vehicle drift. However, the OEM was only able to obtain the specification drawing of the tire and not the Pacejka model from the manufacturer. Rather, a Pacejka tire model from a similar tire was used as the backbone of the model and altered to fit the nominal values as specified by the specification drawings.

The data from the similar tire was obtained from Morencys paper [24]. An extensive spreadsheet was generated to retain the general properties of the tire model while changing the parameters to the specified values. Since all of the parameters are related to each other,

Table 4.2: Steering system friction parameters.

Parameter	Value
Mu Static	0.5
Mu Dynamic	0.5
Friction Force Preload [N]	0.0
Max Friction Force [N]	10000

in order to change certain parameters without affecting other tire properties, built-in scale factors were used. The PAC2002 tire model has 3 scale factors: Lateral force cornering stiffness scale factor γK_y, lateral force horizontal shift scale factor γH_y, and lateral force vertical shift scale factor γV_y. As expected, the lateral force cornering stiffness scale factor alters the cornering stiffness of the tire. The lateral force horizontal shift scale factor shifts the lateral force curve along the x-axis defined as the slip angle γ. In other words, it modifies the value of the slip angle at which zero lateral force is generated, and is used to tune the plysteer lateral forces of the tire. Similarly, the lateral force vertical shift scale factor shifts the lateral force curve along the y-axis defined as the lateral force F_y. In other words, it changes the value of lateral force generated at zero slip angle, and is used to tune the conicity lateral forces of the tire. The cornering stiffness scale factor modifies the slope of the linear region of the lateral force curve and affects the tire's capability to generate lateral forces at a certain slip angle. Within Adams/Car, the program has the ability to mirror the tires to offset the plysteer and conicity tire lateral forces. However, it was found that the function did not work as anticipated and instead, separate left and right tire models were generated to correct this. To generate left and right tire models, the signs of the parameters $pHy1$ and $pVy1$ were modified. It was found that for a negative

plysteer lateral force, the $pHy1$ parameter was negative for a right tire, and positive for a left tire. Since the subject tire had a designed conicity of zero, the parameter $pVy1$ was left unchanged as zero.

4.3.6 Chassis

The chassis only contains a single point mass element. To determine the mass and the location of the chassis, the front and rear wheel weights that were given by the OEM engineers were used in this determination as listed in Table 4.3.

Table 4.3: Vehicle front and rear axle weights

Parameter	**Value**
Vehicle Weight - Front Axle [N]	12199
Vehicle weight - Rear Axle [N]	9638

The chassis was given an arbitrary location with the correct height and a mass that was a bit less than the given value. The model was then fully assembled and tested to tune the location and mass of the chassis in order to achieve the given front and rear wheel weights. Table 4.4 details the final location and mass of the chassis.

Table 4.4: Chassis mass and centre of gravity information after tuning.

Parameter	**Value**
CG Location Behind the Front Axle [mm]	1271
Chassis Mass [kg]	1852

4.4 Model Tuning

This section will illustrate the various simulation tests that were performed to ensure that the model behaved in an expected and predictable manner. Although the model was designed mostly using the specifications provided by the manufacturer, minor modeling issues may arise from incompatible components, assemblies or possibly human error during the modeling process. Two types of tests were identified to tease out such issues: Static suspension simulations that test the full range of motion of the each system, and quasi-static straight-line driving test to check for irregularities in simple vehicle manoeuvres.

Three static suspension tests were available in Adams/Car that allowed the user to analyze the characteristics of a suspension change throughout the vertical range of motion: Opposite wheel-travel analysis, parallel wheel-travel analysis and the single wheel-travel analysis. Of the three analyses, opposite wheel and parallel wheel-travel analyses were performed on the front and rear suspension. Both of the tests required a suspension assembly which includes a suspension system, steering system, and the anti-roll bar system. The analysis attaches actuators to the wheel centre attachment point on the hub of the suspension assembly and displaces it vertically while holding the suspension at the chassis attachment points. The program automatically sets the ride height of the wheel centre pre-determined from the installed length of the spring-damper system. In other words, the installed length of the spring-damper system is the compressed length of the system when the vehicle is not in motion while on flat ground. This installed length can be manually calculated by determining the amount of static spring compression from the weight of the vehicle, or can be automatically calculated by the program. In this model, an installed length was given by the manufacturer, which was 195 millmetres for the front spring/dampers and 221.5 millmetres for the rear spring/dampers. From this position,

the actuators would displace the wheel centre vertically upwards from its lowest position based on the suspensions *rebound* and *jounce* values. The rebound of a suspension is the maximum downward displacement at ride height, and likewise, the jounce of a suspension is the maximum upward displacement.

The parallel wheel-travel analysis displaces both the left and right wheel simultaneously in the same direction. This analysis is particularly useful in identifying binding issues with the suspension, as suspension binding would often cause an irregular bump in the force versus displacement graph as measured at the wheel centre. Binding issues are generally caused by lock-ups in the geometry of the suspension.

As the name suggests, the opposite wheel-travel analysis displaces the left and right wheel simultaneously in opposite directions. This analysis is useful in identifying binding issues with the anti-roll bar system and would be evident in the force versus displacement graph. A screenshot of the setup page from the wheel travel analysis is illustrated in Figure 4.6.

For the front suspension, the jounce and rebound values were set to 86 millmetres and 84 millimetres of displacement respectively, as determined from the manufacturers assembly drawing specification. The jounce and rebound values were not given for the rear suspension, and as such, 50 millimetres of travel were used for both inputs as most modern passenger vehicles would have smaller vertical displacements in the rear suspension.

A force versus vertical displacement graph was plotted from the results of the parallel wheel-travel and opposite wheel-travel analyses for the front and rear suspension. The graphs for the front suspension, as shown in Figure 4.7 and Figure 4.8, illustrate a linear relationship between force and displacement, which indicated that there were no apparent binding issues with the front suspension assembly or with the anti-roll bar system. Likewise,

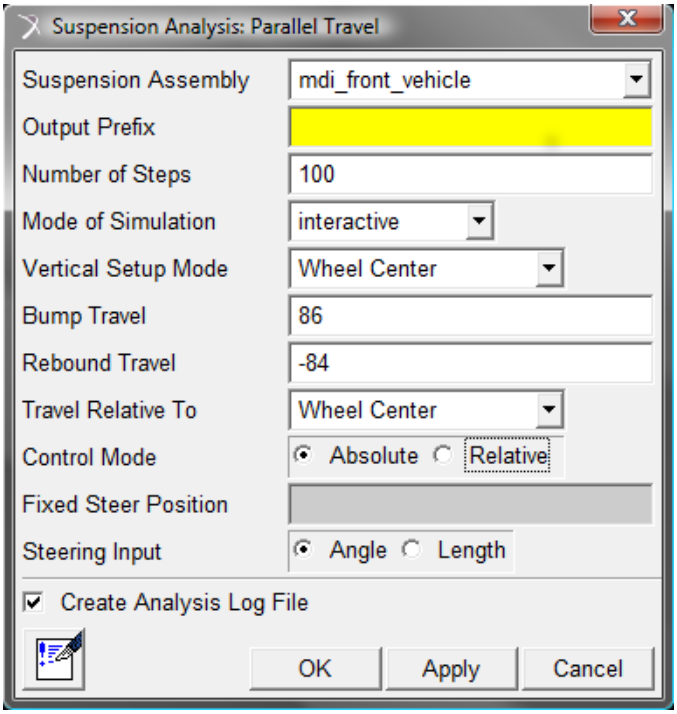

Figure 4.6: Wheel travel analysis input page from Adams/Car.

the graphs for the rear suspension, as shown in Figure 4.9 and Figure 4.10, did not indicate any binding issues. As such, it can be concluded that the front and rear suspension system models would perform as designed in static and quasi-static simulations.

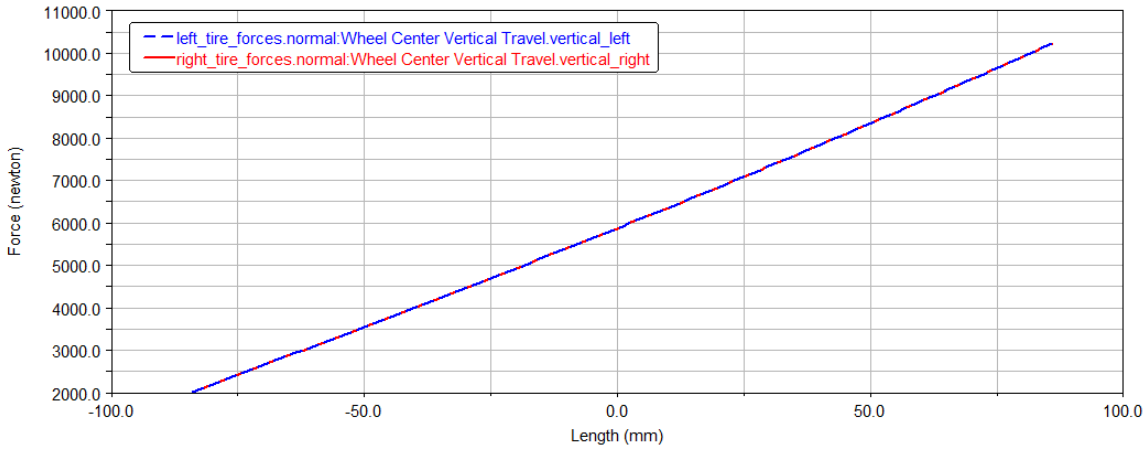

Figure 4.7: Front suspension parallel wheel-travel analysis

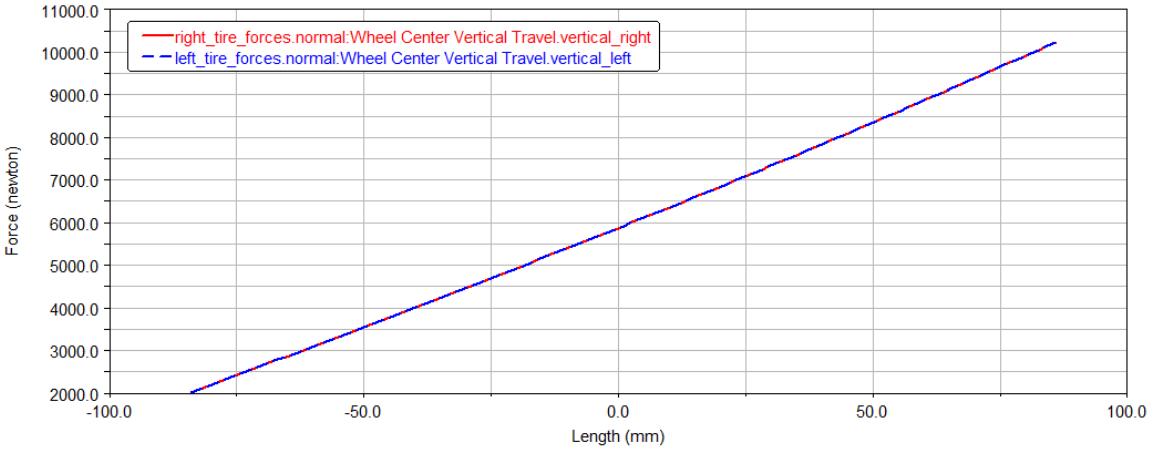

Figure 4.8: Front suspension opposite wheel-travel analysis

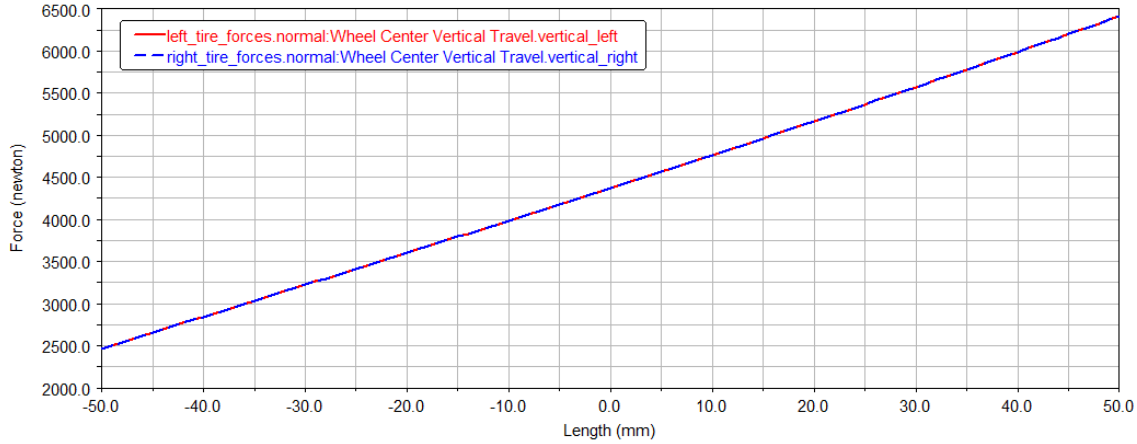

Figure 4.9: Rear suspension parallel wheel-travel analysis

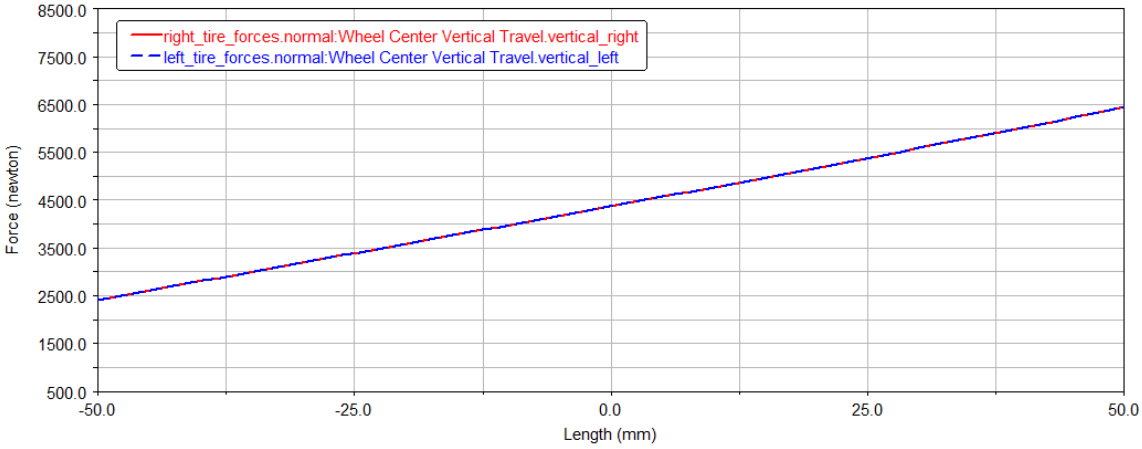

Figure 4.10: Rear suspension opposite wheel-travel analysis

Chapter 5

Vehicle Drift Simulation

This section will describe the vehicle drift simulation based on the industry standard vehicle drift testing. The simulation consisted of a road model, which was created using the Adams/Road plug-in within Adams/Car. The plug-in allowed the user to design custom roads with bank angles. Also, a simple controls model was created in order to emulate the motion required in the drift test. Various simulations were run using the fully built full-vehicle high-fidelity vehicle model based on various road geometry and tire lateral forces. Results of the simulations are discussed within this section.

5.1 Industry Standard Drift Testing

The purpose of the vehicle drift test is to determine the lateral deviation of road vehicles when driven straight, as perceived by the driver. A typical driver would expect their vehicle to drive straight as long as the steering wheel is centred. However, recall that there are numerous factors that may affect the straight-line performance of a vehicle, including the

tire properties, vehicle suspension properties, and road properties. Although the model created in this work can predict and test vehicle drift, automotive engineers were not provided with such a tool in the past, and thus have resorted to physically testing the road vehicles in order to quantify its straight-line performance.

The drift testing begins by accelerating the vehicle to 100 km/h and holding the vehicle's speed constant. The test driver would either try to align the vehicle's longitudinal trajectory along a straight line marked on the test road, or use a measurement tool to determine that the vehicle is tracking straight without any yawing (i.e. zero yaw rate). Once the vehicle is deemed to be driving straight, the test driver would take his or her hand off of the steering, thus removing any steering input from the driver. The vehicle is allowed to drive for more than 100 metres at the same constant speed without any further input. The total vehicle drift is measured from the point in time when the test driver removed any steering input to 100 metres from that point. Figure 5.1 illustrates the test.

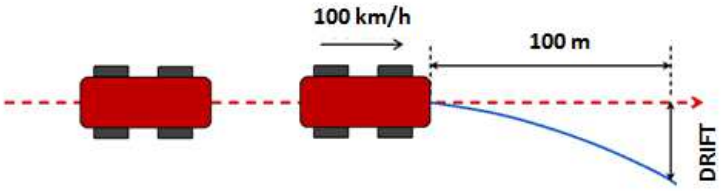

Figure 5.1: Industry standard drift test

5.2 Full-Vehicle High-Fidelity Model Drift Simuation

A vehicle drift simulation of similar nature does not exist within Adams/Car. Rather, a custom simulation was created using the **Event Builder** function within the program.

This function allows the user to manually create a series of events, supplemented by a driver controls model. This is especially useful as the industry standard drift testing that is being emulated contains two separate events: A *straight-line* event to align the vehicle straight, and the *pull test* event to release the steering wheel while keeping the vehicle speed constant. The following sections will detail the road model, the driver controls model, and how they play into the creation of the custom vehicle drift test simulation.

5.2.1 Road Model

As mentioned previously, the road model was created in the **Road Builder** function within Adams/Car. This function allowed the user to create multiple sections of a road with dissimilar geometry and properties. The road friction, road bank angle (the angle at which the road is elevated) and the road width can be varied along the length of the road. The Road Builder also contained a *transition* function that can automatically generate a length of road to join two dissimilar road geometries. This was particularly useful for the banked road model as it comprised a flat section at the start of the road and a banked section at the end. It was found that the vehicle model was sensitive to non-flat roads at the start of the simulation and had difficulty converging. Thus, a flat section of the road was placed at the start of the simulation to allow the simulation to converge.

As shown in Figure 5.2, the road builder did not require the manual generation of road points, but rather, allowed the user to generate sections of the road by specifying its width, bank angle, and friction. The road that was generated for the vehicle drift simulation had three distinction sections: A flat segment, a transition segment, and the banked segment. The flat portion of the road allowed the model to converge properly, while the transition segment gradually changed the road geometry to the banked segment. The banked road

was angled relative to the true ground, which is perpendicular to the direction of gravity.

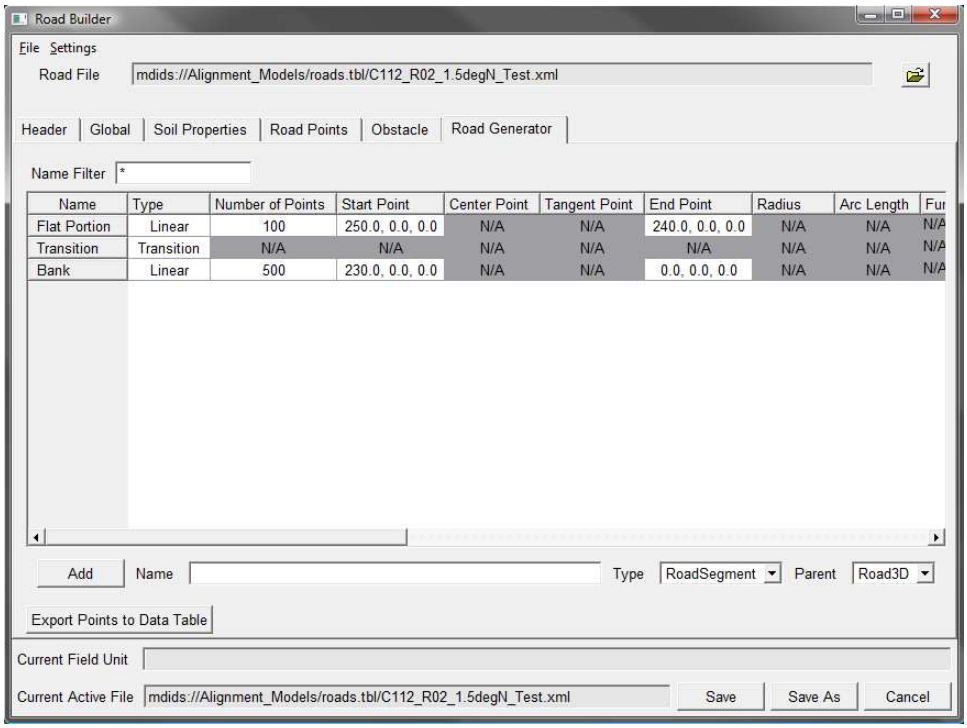

Figure 5.2: Road Builder in Adams/Car

5.2.2 Driver Controls Model

To emulate the test driver performing the standard drift test, a driver controls model was created within the Event Builder. Recall that the first part of the standard test was to hold the vehicle straight at constant speed before releasing the steering. Thus, the controls model will be required to maintain the speed of the vehicle while adjusting the steering to maintain a straight path. Conveniently, Adams had a *straight* function in its steer control module that will be discussed in the following section. The controls module had inputs for its PID inputs for steering, speed and path controls, but was left to default values as it was

not important to emulate a human driver's response. Figure 5.3 and Figure 5.4 illustrates the default values that were used.

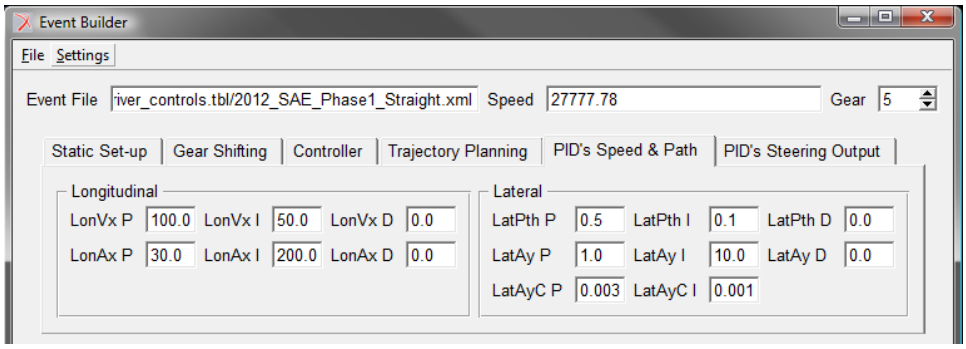

Figure 5.3: PID settings for speed and path tracking

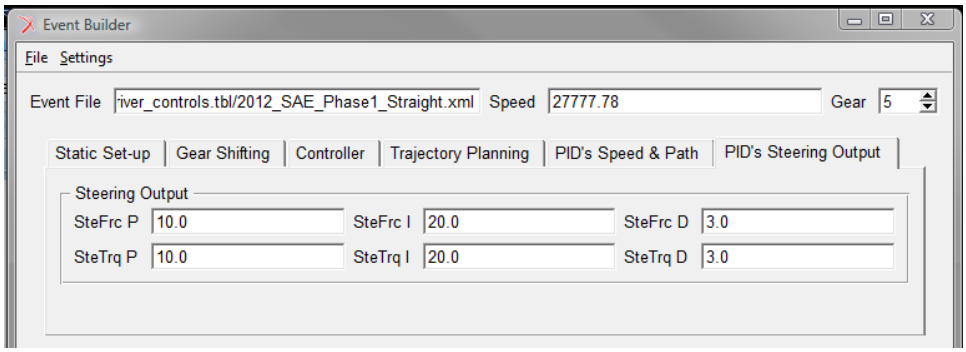

Figure 5.4: PID settings for steering control

5.2.3 Event Builder

The Event Builder combines all of the inputs into an efficient GUI (Graphical User Interface). With the road model created and the driver controls module set, the various events, known as mini-manoeuvres in Adams/Car, were designed to emulate the standard vehicle test motions. At the start of the simulation, the model was allowed to settle and

remove initial transients. Adams/Car offers various methods to specify the static-setup of the analysis, ranging from *normal*, *skidpad* and *straight*, but *settle* was chosen as it allowed the simulation to converge quicker. This method locks the body's fore-aft, lateral, and yaw displacement using joints and performs a static equilibrium to settle the vehicle on the road. Then, before executing the first mini-maneuver, Adams deactivates the joints. For example, selecting settle is equivalent to driving a stake vertically through the vehicle body and constraining the body to move vertically about the stake. It allows the vehicle to roll and pitch, but does not allow rotation about the axis of the stake. When the vehicle is released from this condition, it should be relatively well balanced to remove initial transient effects.

The next mini-manoeuvre required the vehicle to reach a quasi-static state where it would be driven at a constant speed of 100 km/h while maintaining a straight path, or no yaw. This was accomplished by creating a **straight** mini-manoeuvre with *straight* steering control, actuated by rotation rather than torque. Either actuation methods (i.e. rotation or torque) achieved the same results, but it was found that the rotation actuation method reached a straight-line travel quicker than the other methods. It is also important to note that the **control mode** was set to *absolute* to maintain a straight path relative to absolute coordinates, rather than relative to the starting conditions as set by initially settling the vehicle. Also, a speed control was utilized to maintain the vehicle speed at 100 km/h. Screenshots of this mini-manoeuvre in the Event Builder module is shown as Figure 5.5 and Figure 5.6.

The last mini-manoeuvre required the release of the steering wheel while maintaining constant speed. The same speed control was utilized, but steering control was deactivated. This was particularly tricky in Adams/Car, as it is important to input the correct parameters. The actuator type was changed to *torque*, with an *open* control method with a

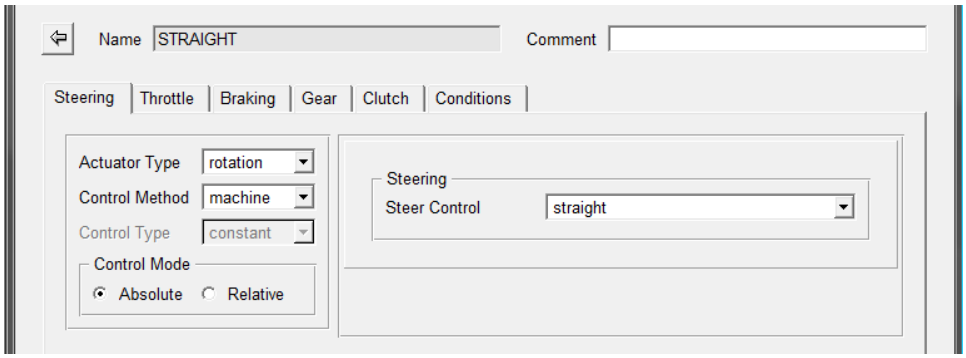

Figure 5.5: Straight-line mini manoeuvre - Steering control

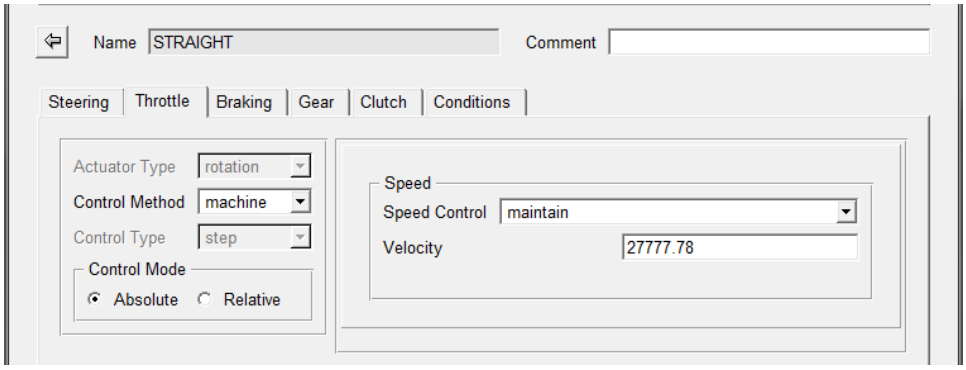

Figure 5.6: Straight-line mini manoeuvre - Speed control

value of zero. Similarly, the torque input was based on absolute values and not relative to the initial conditions. Screenshots of this mini-manoeuvre in the Event Builder module is shown as Figure 5.7.

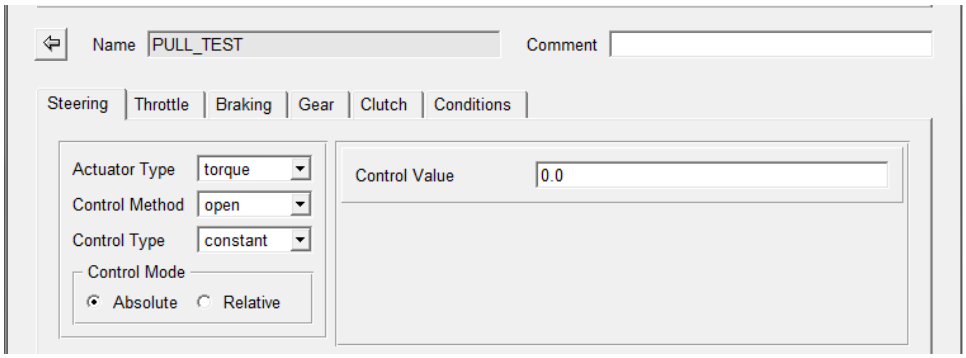

Figure 5.7: Pull-test mini manoeuvre - Steering control

This analysis was aborted after ten seconds of simulation time, which was enough for the vehicle to cover the required 100 metres during the steering release event. The entire simulation and its mini-manoeuvres are illustrated as Figure 5.8.

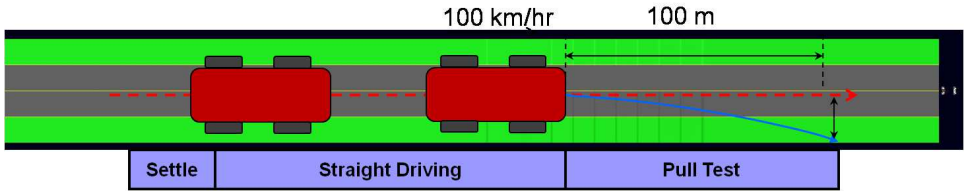

Figure 5.8: Drift test simulation

5.3 Simulation Results

With the full-vehicle model completed and the drift testing analysis designed, a series of simulations were run to understand the effect of suspension properties. Also, simulation

results were compared with the drift testing data gathered by the OEM.

5.3.1 Suspension Geometry Simulations

Recall that the literature reviewed within this thesis revealed that certain suspension parameters had various effects on vehicle drift, namely toe angle, camber angle, and cross camber angle. Although the vehicle models used in the reviewed literature are different than the one designed for this thesis, results should be comparable. A series of simulations were run with the full-vehicle model. Each set of simulations varied one parameter within reasonable physical limits, while the other parameters were set to their nominal values. However, the tire models were altered slightly to produce zero conicity and plysteer forces so the effect of each parameter would not be washed out. The parameters that were varied were front and rear camber, and front and rear toe. Also, the vehicle drift was normalized consistently for all suspension parameter plots, as we are mainly concerned with the relative effect of each parameter.

The front camber was varied by 1 degree of camber from its nominal value of -0.67 degrees. As shown in Figure 5.9, an increase in camber angle from the nominal value increased the vehicle drift to the right (a positive value indicates a vehicle pull to the right). This differs from the results given by Oh *et al.* [28] The authors of the paper had a significant pull to the right with a decrease of 0.5 degrees of camber from nominal. Unfortunately, the paper did not indicate the nominal camber angle used in their vehicle model. Also, the magnitude of pull is much greater. It is likely that *Oh's* tire residual lateral forces have a greater sensitivity to changes in camber. Without knowing the original tire properties, a definitive conclusion cannot be made.

Similarly, the rear camber was varied by 1 degree of camber from its nominal value of

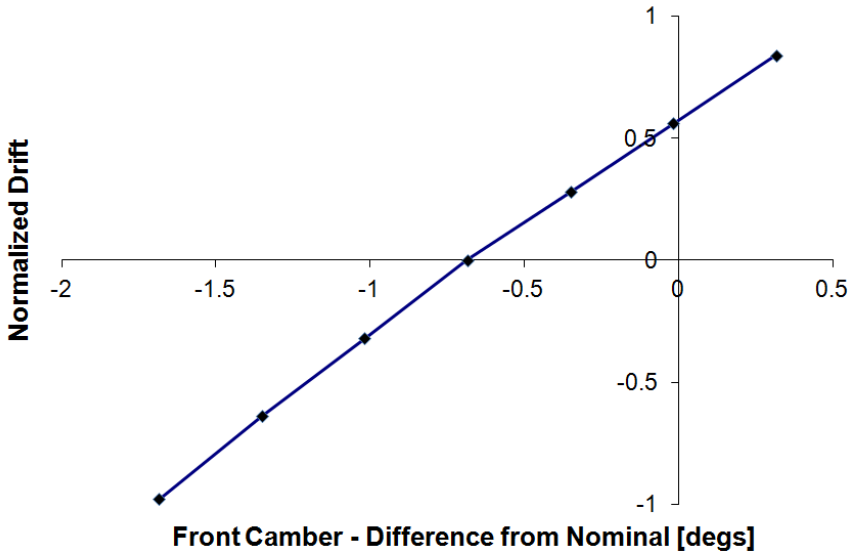

Figure 5.9: Simulation front camber angle results

-0.5 degrees. As shown in Figure 5.10, an increase in camber angle from the nominal value increased the vehicle drift to the left. This differs from the front camber simulation results, which had a pull to the right. Comparing the results contained within the paper by Oh *et al.* [28], the results are similar as the paper had a vehicle drift of 14 millimetres to the left with an increase of 0.5 degrees of rear camber. The results are as expected since an increase in camber angle increased the tire's residual lateral force in the right directions, or along the positive *y-axis*. When the front tires have a positive tire force to the right, the vehicle would tend to crabwalk and rotate to the right. However, when the rear tires have a positive force to the right, the vehicle would still tend to crabwalk to the right, but rotate to the left, thus steering the vehicle left.

The front and rear toe angles were also varied from their nominal value of zero degrees by 0.1 degrees, as shown in Figure 5.11 and Figure 5.12. Like the results shown in the paper by Oh *et al.* [28], the change in toe angles had a negligible effect on vehicle drift,

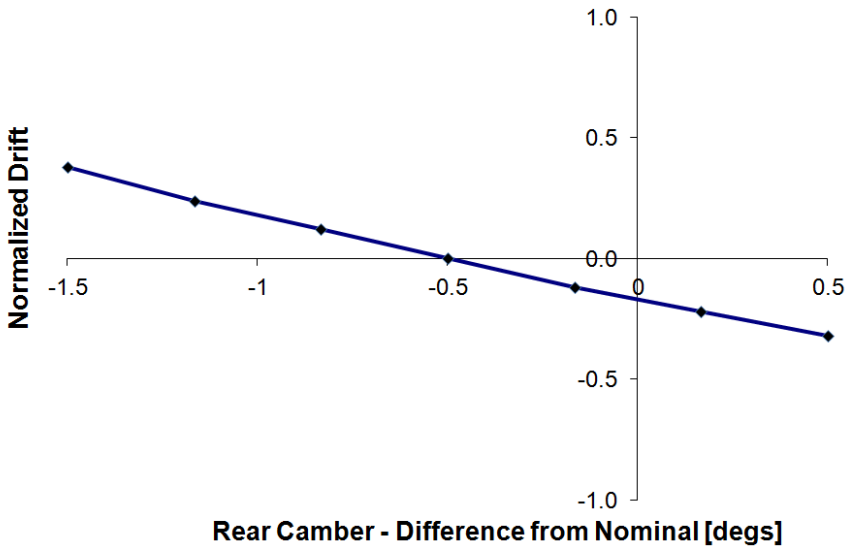

Figure 5.10: Simulation rear camber angle results

and the small variations are likely due to solver tolerances.

5.3.2 Banked Road Simulations

A series of banked road simulations were run with the full-vehicle model for the purpose of comparing the results obtained by the OEM from their physical vehicle drift testing. Seven roads with various road bank or crown angles (-1.5, -0.75, -0.5, 0, +0.5, +0.75, +1.5) were simulated with the full-vehicle model. The sign convention for road bank angles used by the OEM is defined as such: A negative angle slopes toward the left and a positive angle slopes toward the right. All model parameters were set to their nominal values, with the default tire model generating nominal plysteer and conicity forces. The results, as shown in Figure 5.13, indicate that the direction of vehicle pull matches with OEM test data, but the magnitudes differ in both the positively and negatively banked road simulation results. Note that the values in the y-axis are masked to preserve confidentiality.

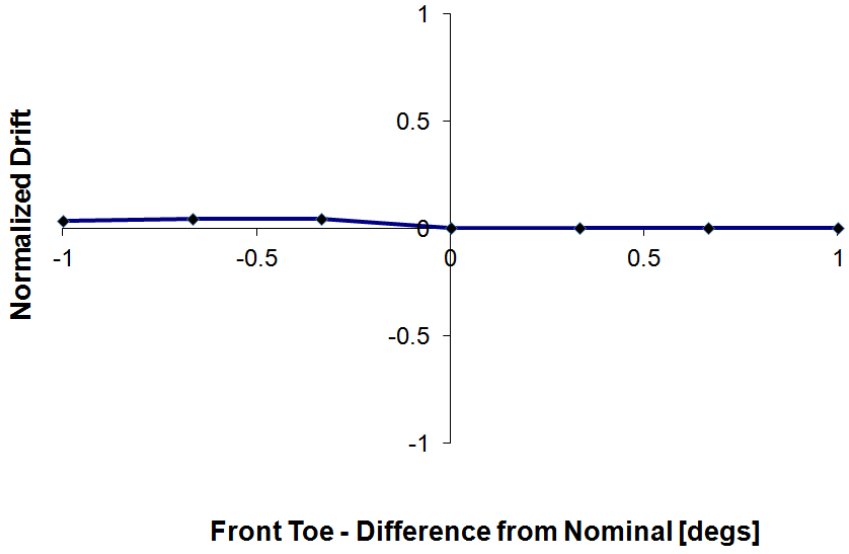

Figure 5.11: Simulation front toe angle results

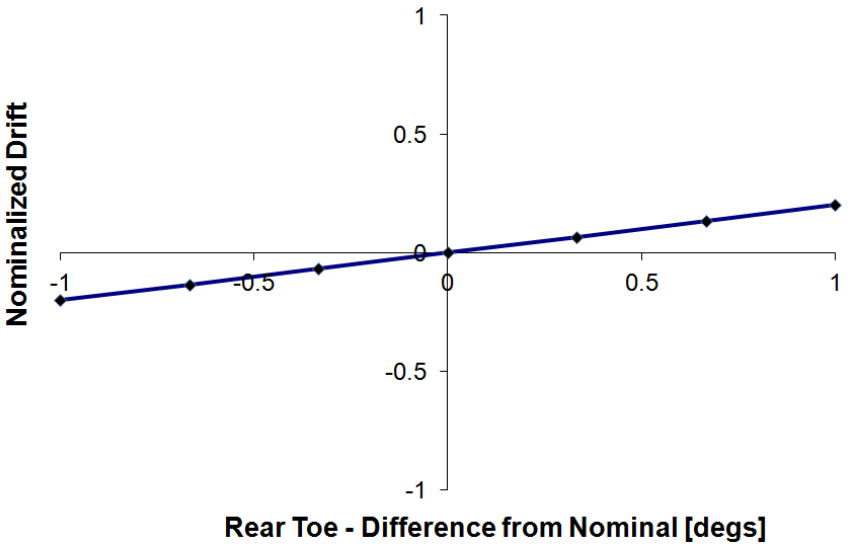

Figure 5.12: Simulation rear toe angle results

It is likely that the difference in vehicle drift is due to the lack of steering data obtained for the full-vehicle model. It was found that the steering friction, steering torsion bar stiffness and damping rate significantly affected the simulated vehicle pull. However, without having the nominal values for these parameters, useful simulation results could not be obtained. Tuning of the steering parameters is an alternative option, but this was outside the scope of this thesis.

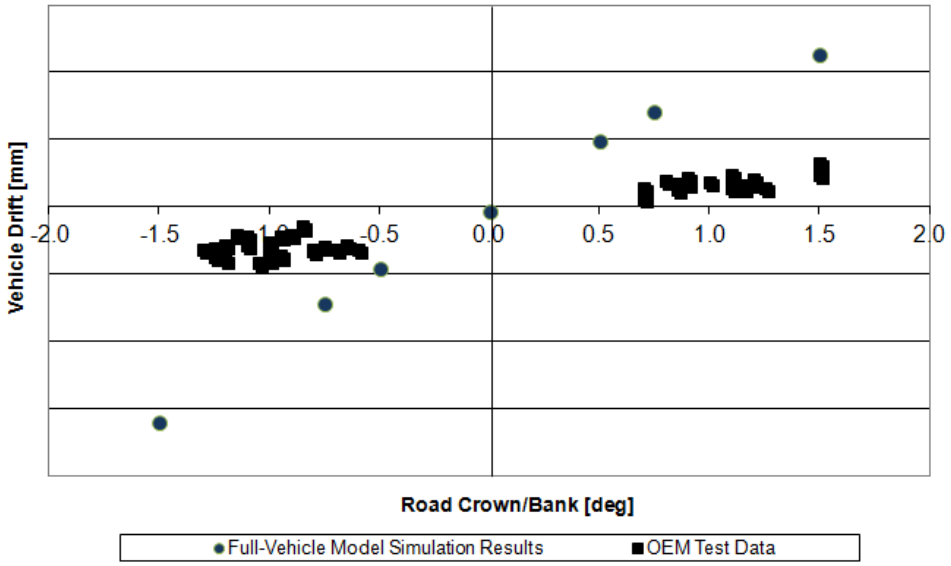

Figure 5.13: Simulation results for banked roads

Chapter 6

Conclusions

MSC.Adams was chosen as the multi-body dynamics software for this research for its ability to develop a model without the initial need for physical test data. A high-fidelity full-vehicle model of the sports utility vehicle (SUV) was successfully created by the software package from data gathered from assembly and component drawings provided by the OEM.

Within the model, the front MacPherson strut and the rear multi-link suspension sub-assemblies were generated by customizing existing suspension sub-assembly templates in Adams/Car to include the appropriate joints and suspension links. Completeness and accuracy of the generated models were heavily dependent on the provided information. Full hardpoint data was completely derived from assembly and component drawings, whereas the inertial properties of the suspension components were partially estimated by Adams/Car given their rough geometries and material properties.

Models were created in Adams 2010 and MapleSim, a multi-body dynamics software that formulates equations of motion based on a body fixed coordinate system, to verify the use of PAC2002 tire models generated by a custom spreadsheet. The first model,

as described in this thesis as the tire test rig model, is a 1-DoF model designed to test and analyze tire models. It was found that the predicted normal and lateral forces at a pre-determined lateral slip angle matched well between the spreadsheet and the two MBD software. Thus, the results provides confidence to the usage of Pacejka tire models for the full-vehicle model. The other model, designated as the 6/7-DoF model, was used to test and verify the effect of the tire residual lateral forces. It was concluded that the generated tire model's behaviour was consistent between two multi-body dynamics software packages.

The full-vehicle model was verified using the parallel wheel travel and opposite wheel travel suspension analyses. The parallel wheel travel analysis was used to tease out binding issues within the designed travel of the suspension, whereas the opposite wheel travel analysis was used similarly for anti-roll bar systems. The resultant data indicates that the model was free of binding issues.

Simulations based on the industry standard vehicle drift testing, were run to understand the effect of certain vehicle suspension geometry on vehicle drift, namely the vehicle's front and rear camber and toe angles. It was found that the camber angle or inclination angle of the suspension increased vehicle drift in the expected direction of travel. However, the toe angle had an insignificant influence on vehicle drift. The full-vehicle model was also subjected to straight-line performance simulations with various road bank or crown angles. The results were compared with the data gathered by the OEM's tests based on industry standards for vehicle drift testing. Upon comparison, it was revealed that the direction of vehicle pull matched the OEM's test data, but the magnitudes differed in both the positively and negatively banked road simulation results. It was postulated that the difference in vehicle drift was likely due to insufficient and/or inaccurate steering data obtained for the full-vehicle model.

The full-vehicle model created in MSC.Adams offers a simulation platform that has the

ability to allow engineers to predict the drift characteristics of a road vehicle. However, additional work is recommended to further increase the accuracy the model's prediction. Full-vehicle testing, such as four-post testing and kinematics and compliance testing, can be done to further optimize the tire and suspension parameters to fully match the vehicle's behaviour. Also, vehicle drift test results can further correlate the model with additional tuning. Nonetheless, a base line high-fidelity model of the SUV was completed using an industry accepted multi-body dynamics software, MSC.Adams, with preliminary results indicating good correlation to peer-reviewed published literature.

References

[1] AASHTO. *A Policy on Geometric Design of Highways and Streets 2011*. AASHTO, sixth edition, 2011.

[2] C.M. Andersen A.K. Noor. Finite element modeling and analysis of tires. *Tire Modeling*, 1982.

[3] I. T. Bruulsema. *Dynamic modeling and design optimization of automotive suspension systems*. PhD thesis, University of Waterloo, 2000.

[4] S.I. Kim B.S. Kim, J.H. Kim. Vehicle drift investigation during straight line accelerating and braking. *SAE Technical Paper Series*, (SAE 2008-01-0588), 2008.

[5] S. Chae. *Nonlinear finite element modeling and analysis of a truck tire*. PhD thesis, The Pennsylvania State University, 2006.

[6] AGCO Automotive Corporation. Roads lean toward the drainage so that water will run off, 2011.

[7] Mechanical Simulation Corporation. Computer simulation of vehicle dynamics for ride, handling, braking, and acceleration of cars, trucks, motorcycles, and motorsports with windows os and real-time systems. http://www.carsim.com/, June 2013.

[8] MSC Software Corporation. *Adams/Car help*, 2010.

[9] MSC Software Corporation. *Adams/Car Ride Help*, 2010.

[10] MSC Software Corporation. *Adams/SmartDriver Help*, 2010.

[11] MSC Software Corporation. *Adams/Tire Help*, 2010.

[12] MSC Software Corporation. Adams: The multibody dynamics simulation solution. http://www.mscsoftware.com/product/adams, June 2013.

[13] MSC Software Corporation. Adams/car: Real dynamics for vehicle design and testing. http://www.mscsoftware.com/product/adamscar, June 2013.

[14] MSC Software Corporation. Maplesim online help - fiala, June 2013.

[15] D.L. Metz D. Milliken, W.F. Milliken. *Race car vehicle dynamics*. SAE International, Warrendale, PA, 1995.

[16] Mechanical Dynamics Inc. *Adams/Pre 11.0 Reference Guide*, 2001.

[17] J. Betzler J. Reimpell, H. Stoll. *Automotive chassis: engineering principles*. Butterwrth-Heinemann, Woburn, MA, 2001.

[18] R. N. Jazar. *Vehicle Dynamics: Theory and Application*. Springer, New York, NY, 2008.

[19] T. David K. Van Gorder. Vehicle dynamics fingerprint process. *SAE Technical Paper Series*, (SAE 1999-01-0117), 1999.

[20] J-H. Lee. Analysis of tire effect on the simulation of vehicle straight line motion. *Vehicle system dynamics*, 33(6):373–390, 2000.

[21] B.E. Lindenmuth. Tire conicity and ply steer effects on vehicle performance. *SAE Technical Paper Series*, (SAE 740074), 1974.

[22] Maplesoft. Maplesim. http://www.maplesoft.com/products/maplesim/, June 2013.

[23] J.J. McPhee. Graph-theoretic modeling of mechanical systems. *Course and class notes for SYDE 652*, 2011.

[24] K.W. Morency. Automatic generation of real-time simulation code for vehicle dynamics using linear graph theory and symbolic computing. Master's thesis, University of Waterloo, Waterloo, ON, 2007.

[25] Society of Automotive Engineers. Vehicle dynamics terminology. (SAE J670), 1998.

[26] H. Pacejka. *Tyre and vehicle dynamics*. Butterworth-Heinemann, Burlington, MA, 2005.

[27] M. Wajroch S.W. Lee R. Mundl, M. Fischer. Simulation and validation of the ply steer residual aligning torque induced by the tyre tread pattern. *Vehicle System Dynamics*, 43(sup1):434–443, 2005.

[28] G. Gim S-H. Oh, Y-H. Cho. Identification of a vehicle pull mechanism. Seoul, 2004. FISITA World Automotive Congress.

[29] M.W. Sayers and D-K. Han. A generic multibody vehicle model for simulating handling and braking. *Vehicle system dynamics*, 25(S1):599–613, 1996.

[30] A. Millie P. Schweizer J.C. Gerdes S.L. Miller, B. Youngberg. Calculating longitudinal wheel slip and tire parameters using gps velocity. In *American Control Conference. Proceedings of the 2001*, volume 3, pages 1800–1805, Arlington, VA, 2001. IEEE.

[31] T. Sutherland W.C. Mitchell, R. Simons and M. Keena-Levin. Suspension geometry: theory vs. K&C measurement. *SAE Technical Paper Series*, (SAE 2008-01-2948), 2008.

APPENDICES

Appendix A

Tire Data

A.1 Tire Data

Tire Property File Format			
Parameter Name	**Units:**	**Value:**	**Description**
	Unitless	4	Tire mode
	m/s	22.2	Tire measurement speed

Dimensions			
Name:	**Units:**	**Value:**	**Description**
R0	m	0.355	Free tire radius
	m	0.235	$Nominal section width of the tyre
	Unitless	0.6	$Nominal aspect ratio
	m	0.229	$Nominal rim radius
	m	0.178	$Rim width
	Pa	200000	Inflation pressure
	Pa	200000	Nominal inflation pressure

Normal Load and Rolling Radius Parameters			
Name:	**Units:**	**Value:**	**Description**
Cz	N/m	210000	Tire vertical stiffness (if qFz1 =0)

Kz	N*s/m	50	Tire vertical damping
BReff	m	8.4	Low load stiffness effecrtive rolling radius
DReff	m	0.27	Peak value of effective rolling radius
FReff	m	0.07	High load stiffness effective roiling radius
Fz0	N	6100	Nominal wheel load at testing
qFz1	Unitless	0	Tire vertical stiffness coefficient (linear)
qFz2	Unitless	0	Tire vertical stiffness coefficient (quadratic)
qFcx1	Unitless	0	Tire stiffness interaction with Fx
qFcy1	Unitless	0	Tire stiffness interaction with Fy
qFc1	Unitless	0	Tire stiffness interaction with camber
qV1	Unitless	0	Tire radius growth coefficient
qV2	Unitless	0	Tire stiffness variation coefficient with speed

Scaling Factors Coefficients for Pure Slip			
Name:	**Units:**	**Value:**	**Description**
Fzo	Unitless	1	Scale factor of nominal (rated) load
Cz	Unitless	1	Scale factor of vertical tire stiffness
Cx	Unitless	1	Scale factor of Fx shape factor
ux	Unitless	1	Scale factor of Fx peak friction coefficient
Ex	Unitless	1	Scale factor of Fx curvature factor
Kx	Unitless	1	Scale factor of Fx slip stiffness
Hx	Unitless	1	Scale factor of Fx horizontal shift
Vx	Unitless	1	Scale factor of Fx vertical shift
x	Unitless	1	Scale factor of inclination for Fx
Cy	Unitless	1	Scale factor of Fy shape factor
uy	Unitless	1	Scale factor of Fy peak friction coefficient
Ey	Unitless	1	Scale factor of Fy curvature factor
Ky	Unitless	1.286948209	Scale factor of Fy cornering stiffness
Hy	Unitless	-0.431277513	Scale factor of Fy horizontal shift
Vy	Unitless	0	Scale factor of Fy vertical shift
gy	Unitless	1	Scale factor of inclination for Fy
t	Unitless	1	Scale factor of peak of pneumatic trail
Mr	Unitless	1	Scale factor for offset of residual moment

y	Unitless	1	Scale factor of inclination for Mz
Mx	Unitless	1	Scale factor of overturning couple
VMx	Unitless	1	Scale factor of Mx vertical shift
My	Unitless	1	Scale factor of rolling resistance moment

Scaling Factors Coefficients for Combined Slip

Name:	Units:	Value:	Description
x	Unitless	1	Scale factor of alpha influence on Fx
y	Unitless	1	Scale factor of alpha influence on Fx
Vy	Unitless	1	Scale factor of kappa-induced Fy
s	Unitless	1	Scale factor of moment arm of Fx

Longitudinal Force Coefficients at Pure Slip

Name:	Units:	Value:	Description
pCx1	Unitless	1.65	Shape factor Cfx for longitudinal force
pDx1	Unitless	1	Longitudinal friction Mux at Fznom
pDx2	Unitless	0	Variation of friction Mux with load
pDx3	Unitless	0	Variation of friction Mux with inclination

pEx1	Unitless	0	Longitudinal curvature Efx at Fznom
pEx2	Unitless	0	Variation of curvature Efx with load
pEx3	Unitless	0	Variation of curvature Efx with load squared
pEx4	Unitless	0	Factor in curvature Efx while driving
pKx1	Unitless	20	Longitudinal slip stiffness Kfx/Fz at Fznom
pKx2	Unitless	0	Variation of slip stiffness Kfx/Fz with load
pKx3	Unitless	0	Exponent in slip stiffness Kfx/Fz with load
pHx1	Unitless	0	Horizontal shift Shx at Fznom
pHx2	Unitless	0	Variation of shift Shx with load
pVx1	Unitless	0	Vertical shift Svx/Fz at Fznom
pVx2	Unitless	0	Variation of shift Svx/Fz with load
rBx1	Unitless	10	Slope factor for combined slip Fx reduction
rBx2	Unitless	6	Variation of slope Fx reduction with kappa
rCx1	Unitless	1	Shape factor for combined slip Fx reduction
rEx1	Unitless	0	Curvature factor of combined Fx
rEx2	Unitless	0	Curvature factor of combined Fx with load
rHx1	Unitless	0	Shift factor for combined slip Fx reduction
pTx1	Unitless	0	Longitudinal relaxation length at Fznom
pTx2	Unitless	0	Variation of longitudinal relaxation length with load
pTx3	Unitless	0	Variation of longitudinal relaxation length with exponent of load

Lateral Force Coefficients at Pure Slip			
Name:	**Units:**	**Value:**	**Description**
pCy1	Unitless	1.1058	Shape factor Cfy for lateral forces
pDy1	Unitless	1.0491	Lateral friction Muy
pDy2	Unitless	-0.2153	Variation of friction Muy with load
pDy3	Unitless	-0.33848	Variation of friction Muy with squared inclination
pEy1	Unitless	-0.87148	Lateral curvature Efy at Fznom
pEy2	Unitless	-1.5278	Variation of curvature Efy with load
pEy3	Unitless	-0.025987	Inclination dependency of curvature Efy
pEy4	Unitless	0.90729	Variation of curvature Efy with inclination
pKy1	Unitless	-23.648	Maximum value of stiffness Kfy/Fznom
pKy2	Unitless	2.1393	Load at which Kfy reaches maximum value
pKy3	Unitless	-0.90729	Variation of Kfy/Fznom with inclination
pHy1	Unitless	-0.00017802	Horizontal shift Shy at Fznom
pHy2	Unitless	-0.00003498	Variation of shift Shy with load
pHy3	Unitless	0.02906	Variation of shift Shy with inclination.
pVy1	Unitless	0.00000	Vertical shift in Svy/Fz at Fznom
pVy2	Unitless	0.0000	Variation of shift Svy/Fz with load
pVy3	Unitless	0.0000	Variation of shift Svy/Fz with inclination

	pVy4	Unitless	0.0000	Variation of shift Svy/Fz with inclination and load
rBY1		Unitless	16	Slope factor for combined Fy reduction
rBY2		Unitless	0	Variation of slope Fy reduction with alpha
rBY3		Unitless	0	Shift term for alpha in slope Fy reduction
rCY1		Unitless	1	Shape factor for combined Fy reduction
rEY1		Unitless	0	Curvature factor of combined Fy
rEY2		Unitless	0	Curvature factor of combined Fy with load
rHY1		Unitless	0	Shift factor for combined Fy reduction
rHY2		Unitless	0	Shift factor for combined Fy reduction with load
rVY1		Unitless	0	Kappa induced side force Svyk/Muy*Fz at Fznom
rVY2		Unitless	0	Variation of Svyk/Muy*Fz with load
rVY3		Unitless	0	Variation of Svyk/Muy*Fz with camber
rVY4		Unitless	0	Variation of Svyk/Muy*Fz with alpha
rVY5		Unitless	1.9	Variation of Svyk/Muy*Fz with kappa
rVY6		Unitless	0	Variation of Svyk/Muy*Fz with atan(kappa)
pTy1		Unitless	0	Peak value of relaxation length for lateral direction
	pTy2	Unitless	0	Shape factor for lateral relaxation length

Aligning Coefficients at Pure Slip			
Name:	**Units:**	**Value:**	**Description**
qBz1	Unitless	14.973	Trail slope factor for trail Bpt at Fznom
qBz2	Unitless	-3.5918	Variation of slope Bpt with load
qBz3	Unitless	-0.72704	Variation of slope Bpt with load squared
qBz4	Unitless	-0.007765	Variation of slope Bpt with inclination
qBz5	Unitless	-0.00819	Variation of slope Bpt with absolute inclination
qBz9	Unitless	17.781	Slope factor Br of residual moment Mzr
qBz10	Unitless	0	Slope factor Br of residual moment Mzr
qCz1	Unitless	1.132	Shape factor Cpt for pneumatic trail
qDz1	Unitless	0.0000	Peak trail Dpt = Dpt*(Fz/Fznom*R0)
qDz2	Unitless	-0.0026745	Variation of peak Dpt with load
qDz3	Unitless	-0.0066332	Variation of peak Dpt with inclination
qDz4	Unitless	-6.238	Variation of peak Dpt with inclination squared.
qDz6	Unitless	0.00031509	Peak residual moment Dmr = Dmr/ (Fz*R0)
qDz7	Unitless	0.0002961	Variation of peak factor Dmr with load
qDz8	Unitless	-0.081607	Variation of peak factor Dmr with inclination
qDz9	Unitless	-0.08016	Variation of Dmr with inclination and load
qEz1	Unitless	-1.7447	Trail curvature Ept at Fznom
qEz2	Unitless	-0.58532	Variation of curvature Ept with load

qEz3	Unitless	0	Variation of curvature Ept with load squared
qEz4	Unitless	0.0029202	Variation of curvature Ept with sign of Alpha-t
qEz5	Unitless	-2.2229	Variation of Ept with inclination and sign Alpha-t
qHz1	Unitless	0.00025222	Trail horizontal shift Sht at Fznom
qHz2	Unitless	0.000068468	Variation of shift Sht with load
qHz3	Unitless	-0.019273	Variation of shift Sht with inclination
qHz4	Unitless	0.0092761	Variation of shift Sht with inclination and load
sSz1	Unitless	0	Nominal value of s/R0: effect of Fx on Mz
sSz2	Unitless	0	Variation of distance s/R0 with Fy/Fznom
sSz3	Unitless	0	Variation of distance s/R0 with camber
sSz4	Unitless	0	Variation of distance s/R0 with load and camber
qTz1	Unitless	0	Gyroscopic moment constant
Mbelt	kg	5.4	Belt mass of the wheel